

AperTO - Archivio Istituzionale Open Access dell'Università di Torino

Influence of start-up phase of an incinerator on inorganic composition and lead isotope ratios of the atmospheric PM₁₀

This is the author's manuscript

Original Citation:

Availability:

This version is available <http://hdl.handle.net/2318/1783153> since 2021-04-15T22:33:43Z

Published version:

DOI:10.1016/j.chemosphere.2020.129091

Terms of use:

Open Access

Anyone can freely access the full text of works made available as "Open Access". Works made available under a Creative Commons license can be used according to the terms and conditions of said license. Use of all other works requires consent of the right holder (author or publisher) if not exempted from copyright protection by the applicable law.

(Article begins on next page)

1 **Influence of start-up phase of an incinerator on**
2 **inorganic composition and lead isotope ratios of the**
3 **atmospheric PM₁₀**

4 Daniele Ziegler¹, Mery Malandrino^{2*}, Claudia Barolo², Gianpiero Adami³, Milena
5 Sacco⁴, Francesco Pitasi⁴, Ornella Abollino⁵, Agnese Giacomino⁵

6 ¹ Department of Applied Science and Technology, Polytechnic of Turin, Torino I-10129, Italy

7 ² Department of Chemistry, NIS Interdepartmental and INSTM Reference Centre, University of Turin,
8 Torino I-10125, Italy

9 ³ Department of Chemical and Pharmaceutical Sciences, University of Trieste, Trieste I-34127, Italy

10 ⁴ Piedmont Regional Agency for the Environmental Protection, Torino I-10135, Italy

11 ⁵ Department of Drug Science and Technology, University of Turin, University of Turin, Torino I-10125,
12 Italy

13
14 Corresponding author. Mery Malandrino Via P. Giuria 5, 10125 Torino Italy.

15 E-mail address: mery.malandrino@unito.it (M. Malandrino).

16

17 **Abstract:**

18 A municipal solid waste incinerator (MSWI) was installed in a peripheral area of the city of Turin. In this
19 study, we evaluated the contribution of this plant to the massive concentration of PM₁₀, to its chemical
20 composition and to the distribution of the lead isotopes during the start-up phase.

21 We assessed the inorganic composition of PM₁₀ collected in the vicinity of the Turin incinerator by
22 inductively coupled plasma atomic emission spectroscopy (ICP-AES), magnetic sector inductively coupled
23 plasma mass spectrometer (SF-ICP-MS) and ion chromatography (IC). The lead isotope ratios in PM₁₀
24 samples were determined by SF-ICP-MS by a method developed and optimized using experimental design
25 approach.

26 Element trends and data chemometric treatment evidence that the vehicular traffic, increased in this area
27 due to the opening of the MSWI plant, and, to a lesser degree, the direct incinerator emissions influence
28 As, Cd, Cr, Cu, Ba, Mo, Pb, Sn and Zn concentrations. As a whole, however, the element concentrations in
29 PM₁₀ and the Enrichment Factors (EFs) were comparable with the values reported for other urban sites and
30 target pollutant concentrations of MSWI emissions, namely Cd, Cr, Cu and Pb, were lower than in PM₁₀
31 emitted from older MSWIs. This confirms that incinerators of new installation have a lower impact on
32 atmospheric PM₁₀ composition thanks to stricter current legislation and up-to-date technologies. The lead
33 isotope ratios investigation allowed to distinguish the diverse sources (crustal, vehicular traffic and MSWI)
34 that influence lead concentration in PM₁₀ collected near incinerator during start-up phase.

35

36 **Keywords:**

37

38 Incinerator; Trace elements in PM₁₀; Chemometric processing; Lead isotope ratios

39

40 **List of Abbreviations**

41 MSWI Municipal Solid Waste Incinerator

42	IC	Ion Chromatography
43	ICP-AES	Inductively Coupled Plasma Atomic Emission Spectroscopy
44	SF-ICP-MS	Magnetic Sector Inductively Coupled Plasma Mass Spectrometer
45	EFs	Enrichment Factors
46	PM	Particulate Matter
47	WSI	Water Soluble Ions
48	TRM	Trattamento di Rifiuti Metropolitani
49	PCA	Principal Component Analysis
50	HCA	Hierarchical Cluster Analysis
51	CCD	Central Composite Design
52	PLS	Partial Least Square
53	PBL	Planetary Boundary Layer

54

55 **1. Introduction**

56 Air pollution represents one of the greatest concerns of urban environments. During the last decades great
57 attention was paid to Particulate Matter (PM), due to the correlation between fine PM exposure and adverse
58 health effects. The damage to health correlated to PM air pollution is one of the main environmental issues
59 raised by World Health Organization.

60 The Po Valley covers the territory of several regions in Northern Italy and includes many urban
61 agglomerates, such as Turin, Milan, Venice and Bologna. The area is densely populated and heavily
62 industrialized. High amounts of atmospheric pollutants, e.g. about 400.000 tons of NO_x, 80.000 tons of PM
63 and 250.000 tons of NH₃ (ammonia), are emitted per year by a wide variety of pollution sources, which are
64 mainly related to traffic, domestic heating, industry and energy production, agriculture and farming
65 activities (Raffaelli et al., 2020). Furthermore, the geographic conformation prevents an efficient dispersion
66 of primary pollutants and causes a consequent high formation of secondary pollutants. The European

67 Environmental Agency indicated the Po Valley as a hot spot region for air pollutants, in particular for NO₂
68 in 2013 (EEA, 2013 and 2015).

69 The mechanisms responsible for the biological effects of particulate matter have been continuously
70 undergone review, and many questions are still open about some relevant aspects, for example size fraction,
71 number or mass of the particles, chemical components, among which metal elements are relevant species.
72 Metals generally occur as different chemical compounds and in different oxidation states and are distributed
73 among various dimensional fractions of the PM in the troposphere. Transport and distribution of aerosol
74 particles strictly depend on their size, as well as to the weather conditions (Poschl, 2005).

75 Concentration, composition and size distribution of atmospheric particles are temporally and spatially
76 highly variable. Altogether, however, particles size depends primarily on emission sources, and typically
77 those emitted from anthropogenic sources are smaller than those emitted from natural ones (Harrison et al.,
78 2012).

79 On the base of existing scientific evidence, many metals (often depending on their oxidation state) may
80 have a direct or indirect active role in PM biological mechanisms of action.

81 Municipal solid waste incinerators (MSWIs) can be significant sources of atmospheric environmental
82 pollution, potentially exposing nearby populations to hazardous chemicals at toxic levels. Both inorganic
83 and organic chemicals have been identified in MSWI emissions, for instance carbon monoxide (CO), carbon
84 dioxide (CO₂), sulphur oxides (SO_x), nitrogen oxides (NO_x), dioxins and furans, volatile organic
85 compounds (VOC), polycyclic aromatic hydrocarbons (PAHs), metals and particulate matter (PM) (WHO,
86 2007). Some of these chemicals have been classified as known (group 1) or probable (group 2A)
87 carcinogens for humans according to the International Agency for Research on Cancer (IARC, 2012). Some
88 studies have suggested associations between MSWI emissions and health effects, particularly adverse
89 impacts on reproduction and cancer (Vinceti et al., 2008).

90 Because of these troubles that have been identified in earlier studies, more recent investigations have been
91 designed and implemented with the goal of establishing a better definition of exposure and/or effects arising
92 from MSWIs.

93 Directive 2000/76/EC of the European Parliament and the Council on Incineration of Waste enforces
94 measures to prevent or reduce negative effects to the environment, particularly emissions into air, soil and
95 surface water, as well as to human health, which might arise from incineration and co-incineration of waste.
96 More in detail, this directive states that incineration facilities shall be submitted to a permission to operate,
97 which sets rigorous operating conditions, technical requirements and daily emission limits of 10 mg/m^3 for
98 total dust and 0.5 mg/m^3 for the sum of Sb, As, Pb, Cr, Co, Cu, Mn, Ni and V (Directive 2000/76/EC, 2010).
99 When discussing the environmental characteristics of a specific region, the identification of various sources
100 of a pollutant becomes significant; consequently, the MSWI presence must be considered as a possible
101 source of pollutants in airborne particulate matter. The knowledge of the metal content in PM is also
102 important in recognizing its sources since these emit airborne PM with different metal distribution. MSWIs,
103 indeed, play an important role in the treatment of municipal waste according to the recent European
104 directives and it is very important to know the contribution of a MSWI plant of new generation to the
105 inorganic composition of atmospheric PM_{10} . Many studies have evaluated the impact of MSWIs on air
106 quality (Carignan et al., 2005; Pacyna et al., 2007; Font et al., 2015; Panepinto et al., 2018; Lucarelli et al.,
107 2019) but, to our knowledge, none of these has evaluated the contribution during start-up phase.

108 Pb is a poisonous metal that can damage nervous connections especially in young children and cause blood
109 and brain disorders (Tong et al., 2000; Gerhardsson, 2004; Meyer et al., 2008). The concentration of this
110 heavy metal in PM is regulated by the Directive 2008/50/EC, which establishes a limit value of $0.5 \text{ }\mu\text{g/m}^3$
111 for a calendar year (Directive 2008/50/EC, 2008). Although lead occurs naturally in the environment, most
112 of the high levels found throughout the environment derived from human activities. The European Union
113 established the 1st of January 2000, as a limit date to remove leaded fuel from the market, although the
114 European Commission conceded derogation to Spain, Italy and Greece until the 1st of January 2002. That
115 is the reason why the concentration of this element in air has been decreasing since then, although other
116 anthropogenic sources persist, such as smelting, steel mills, incineration of residues, wood and coal
117 combustion, resuspension of contaminated soil dust and industrial activities (production of paintings,
118 chemical agents, welds, etc.) (Widory et al., 2004, 2010; Zhao et al., 2017, 2019; Xu et al., 2020). The

119 identification of stable lead isotope composition in atmospheric particulate matter of several cities around
120 the world is being increasingly used to better characterize atmospheric lead sources (Carignan et al., 2005;
121 Komarek et al., 2008; Guéguen et al., 2012; Gioia et al., 2010, 2017; Zhao et al. 2019; Lee et al., 2019; Xu
122 et al., 2020).

123 This study focuses on:

- 124 • evaluation of the contribution of a new MSWI plant in start-up phase to total PM_{10} and its chemical
125 composition in water soluble ions (WSI) and major, minor and trace elements;
- 126 • development, thorough an Experimental Design approach, of an accurate method for the calculation
127 of lead isotope ratios using microwave acid digestion followed by magnetic sector inductively
128 coupled plasma mass spectrometer (SF-ICP-MS) determination;
- 129 • discrimination between different sources of lead, known to be a marker of incinerator's emission,
130 through a study of its isotope ratios.

131

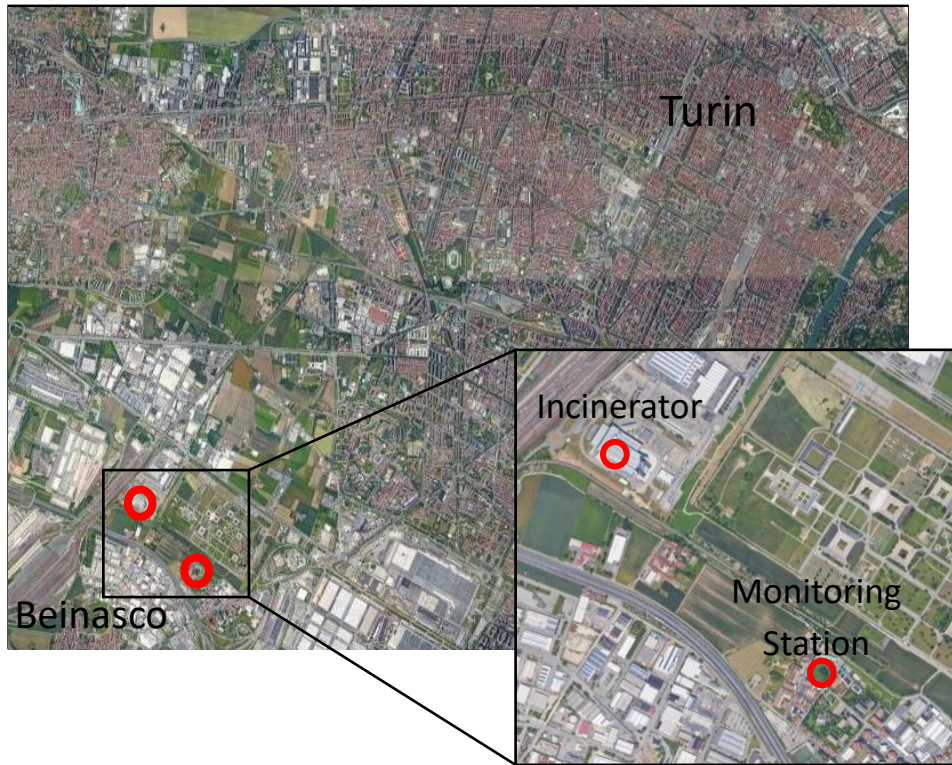
132 **2. Materials and methods**

133 ***2.1 Sampling location and PM_{10} collection***

134 An incinerator was built in the city of Turin, a metropolitan area characterized by many industrial activities
135 and huge volume of vehicular traffic, between 2010 and 2013 and initially was authorized to receive a
136 maximum of 421,000 tons of waste per year from the province of Turin and from other regions. In July
137 2015, following revision of the Integrated Environmental Authorization, the plant's capacity was stepped
138 up to 490,000 tons per year. This plant is precisely located in the south-western zone of Turin outskirts. It
139 converts municipal solid waste, as well as special waste that can be combined with the municipal waste (up
140 to a maximum of 124,000 tons per year), into electrical and thermal energy. More in detail, it consists in a
141 moving grate with four methane burners able to produce 41 MW of electrical power and 106 MW of district
142 heating simultaneously. It is managed by a metropolitan waste treatment society (Trattamento di Rifiuti

143 Metropolitani – TRM S.p.A.); for this reason, the sampling location is hereinafter referred to as TRM
144 (<http://trm.to.it/>).

145 PM₁₀ sampling was carried out in spring and summer 2013 in one site localized near the incinerator, in the
146 area with the highest probability that PM emitted from the plant is falling to the ground. Air quality
147 monitoring station is placed at 45°02'45" N and 7°37'00" E, in the Aldo Mei park of Beinasco town
148 (Province of Turin) and it is managed by Regional Agency for Environmental Protection (ARPA,
149 Piedmont). It is equipped with several instruments (PM₁₀ and PM_{2.5} Beta Attenuation Mass Monitor, Swam
150 5A Dual Channel model, FAI instruments; Analyzer for Nitrogen Compounds, 200E model, Teledyne API;
151 PM₁₀ Sampler, with a Sentinel 96 module for the automatic sequential sampling, Charlie model, TCR
152 Tecora; dioxins/furans Sampler, ECHO HiVol model, TCR Tecora; Wet&Dry Deposimeter Samplers for
153 dioxins/furans and polycyclic aromatic hydrocarbons, Labservice Analytica; Air Mercury Monitor, RA-
154 915 AM model, Lumex) to detect specific air pollutants like NO_x, gaseous Hg, PM₁₀ and PM_{2.5} mass
155 concentrations. A map of the metropolitan area, showing the position of the incinerator and the monitoring
156 station, is reported in Figure 1.



158 *Figure 1: Geographical map of Piedmont and detail of the position of the incinerator and the monitoring*
159 *station.*

160
161 The PM₁₀ samples were collected using a high-volume air sampler (Digitel DHA) and 80 and 150 mm
162 diameter quartz filters to ensure a large amount of PM₁₀ that would allow also the lead isotopic
163 investigation. Sampling duration for each sample was fixed at 24 hours, at a flow of 29 m³/h for a total
164 volume of sampled air of 700 m³.

165 A low volume air sampler, at a flow rate of 2.3 m³/h and equipped with 47 mm diameter quartz filter, was
166 adopted in order to evaluate daily mass concentration of PM₁₀. The flow control was carried out in the
167 actual condition mode and the mass concentrations of PM₁₀ were measured by weighing each filter before
168 and after sampling on an analytical balance in a controlled atmosphere (20 °C, 50% relative humidity)
169 according to Ministerial Decree 60/2002 (D.Lgs. 60, 2002). Meteorological conditions (i.e. average and
170 maximum wind speed, average and maximum mixing height, and average temperature) were obtained from
171 the Minerve calculation model, a diagnostic model for the reconstruction of three-dimensional wind and
172 temperature fields (Table 1S Supplementary Material).

173

174 ***2.2 Choice of PM10 samples***

175 The activity of Turin MSWI plant started on 19th April 2013, by testing the first combustion line. Then,
176 from 22 May to 5 June also the second combustion line began to be active. Subsequently, from 5 June, the
177 second combustion line of the plant was suspended, and it started again the activity in July.

178 Twenty-two samples were chosen for this study in the period between May and July 2013. The choice was
179 performed considering the most representative days, based on the evaluation of two statistical methods:
180 Principal Component Analysis (PCA) and Hierarchical Clustering Analysis (HCA) (shown in figure 1S, 2S
181 and 3S in Supplementary Material).

182 Both meteorological parameters, obtained by a weather station located in the site, such as average and
183 maximum wind speed (m/s), average temperature, average and maximum mixing height, and chemical

184 parameters, such as PM_{10} , $PM_{2.5}$, NO_2 and NO concentrations (Table 1S), were considered, obtaining a
185 dataset composed by 56 samples and 9 variables. These data were supplied by ARPA Piedmont.
186 All chemometric elaborations were carried out after autoscaling of the data. PC1 and PC2 collect the 62.6%
187 (41.6% and 21% respectively) of total variance.
188 More in detail, from loading plot it was clear that both PM_{10} and $PM_{2.5}$ amounts are anticorrelated with
189 wind speed, as expected; as a matter of fact, the samples collected in May are characterized by negative
190 scores values on PC1, suggesting that these samples are most influenced by wind speed variable. This is
191 true especially for samples 25 and 26 May (25/5 and 26/5), two weekend days, when the airborne particulate
192 emitted by tracks is consistently reduced; these samples, together with 29 May (29/5) and 31 May (31/5),
193 show the minimum amount of PM_{10} and, in the score plot, are placed in opposite position to the vector
194 representing this variable.
195 In fact, during May, higher speed of wind values was recorded, resulting in an enhanced dispersion of
196 particulate matter respect to the summer period. Surprisingly, temperature variable is quite correlated to
197 PM_{10} amount in troposphere. This phenomenon can be due to the enhanced rainfall recorded in May,
198 resulting in a decrease of both temperature and coarse fraction of particulate matter. Moreover, NO
199 concentration appears anti-correlated with mixing height. NO presence has an influence in the concentration
200 of NO_2 , that is obtained from the former after a photochemical oxidation in troposphere due to ozone. In
201 the month of May, NO concentration is higher than in June and July, due to the lower height of the PBL
202 (Planetary Boundary Layer). Finally, PM_{10} and $PM_{2.5}$ concentrations are correlated with NO_2 concentration,
203 and they are also anti-correlated with the wind speed as seen in Yadav et al. (2014), describing a more
204 polluted environment for higher PM and NO_2 concentrations. This phenomenon is verified especially for
205 three weekdays, 17, 18 and 19 June (17/6, 18/6 and 19/6), in which samples are characterized by PM_{10}
206 concentrations up to $30 \mu\text{g}/\text{m}^3$ with a reduced transport of particulate matter over long distances.
207 In addition, through HCA three main clusters were detected: a cluster composed by the samples collected
208 at the end of May, displaying lower PM_{10} concentrations and other two clusters comprising the samples
209 from June and July separated according to PM_{10} concentrations and the weather conditions.

210 We chose PM₁₀ samples considering the results obtained from both chemometric techniques: PM₁₀ samples
211 more influenced by PC1 and PC2 and representing evenly the clusters evidenced by HCA were selected.
212 PM₁₀ samples having the highest and the lowest PM₁₀ concentration in each month were also selected. Our
213 selection criterion has permitted us to compare days with a high and a low concentration of particulate
214 matter and to provide information on the dominant sources of atmospheric aerosol in the investigated area,
215 even if we cannot consider this selection as representative of the possible patterns of atmospheric pollutants
216 in the whole period.

217

218 ***2.2 Element and WSI determination***

219 All filters have been analyzed to determine the mass of particulate collected using a gravimetric technique
220 according to Ministerial Decree 155/ 2010 (D.Lgs. 155, 2010).

221 The aerosol-loaded filters (143 mm of the total 150 mm diameter) were punched into 36 mm diameter
222 circular sections. The determination of elements and WSI was executed in duplicate and, for each replicate,
223 two aliquots of each filter were considered. This approach showed that PM₁₀ distribution on filters was
224 equable. In fact, relative standard deviation (RSD) was <10% for all the elements except for potassium with
225 a value equal to 15%.

226 Each sub-sample for element determination was digested by a microwave oven (Milestone-Ethos One) with
227 a mixture of 3.5 mL of sub-boiled HNO₃, 1.5 mL of ultra-pure H₂O₂ (Sigma-Aldrich) and 3 mL of HPW
228 (Milli-Q (Millipore) ultrapure water, resistivity = 18.2 MΩ cm) in 100 mL tetrafluoromethoxyl vessels. The
229 following heating steps were applied: 5 min ramp until 170 °C, 10 min dwell at 170 °C, 5 min ramp until
230 200 °C, 20 min dwell at 200 °C, and 30 min of ventilation. The resulting solutions were filtered on cellulose
231 filters (Whatman Grade 5) to eliminate the undissolved filter parts and diluted to 30 mL with HPW. By this
232 method, the concentrations of trace elements not enclosed in silicate matrix were transferred quantitatively
233 into solution.

234 Elements present in lower concentrations were determined by SF-ICP-MS (Thermo Finnigan Element 2).

235 Mass resolution and isotope selection were optimized for each element to ensure resolution of spectral

236 interferences and maximize sensitivity. The following isotopes of the investigated elements were
237 monitored: ^{47}Ti , ^{48}Ti , ^{51}V , ^{53}Cr , ^{63}Cu , ^{65}Cu , ^{68}Zn , ^{75}As , ^{90}Zr , ^{95}Mo , ^{98}Mo , ^{111}Cd , ^{112}Cd , ^{114}Cd , ^{118}Sn , ^{138}Ba ,
238 ^{207}Pb , ^{208}Pb at low resolution ($R=400$); ^{46}Ti , ^{59}Co , ^{60}Ni , ^{61}Ni , ^{62}Ni , ^{64}Zn , ^{66}Zn , ^{96}Mo , ^{113}Cd , ^{139}La , ^{140}Ce , ^{203}Tl ,
239 ^{205}Tl , ^{204}Pb , ^{206}Pb at medium resolution ($R=4,000$). Analyses on each sample were conducted following a
240 60s uptake and stabilization period. In low resolution 9 replications (3 run x 3 passes) for each selected
241 isotope were carried out, while in medium resolution 12 replications (4 run x 3 passes) for every isotope
242 were carried out. Between samples the nebulizer system was rinsed for 2 min with 2% sub-boiled HNO_3 ,
243 which eliminated carry-over and reconditioned the sampler cone. Power applied was 1270 W, 1 L/min flow
244 of both auxiliary and nebulizer gasses, while plasma gas was fluxed at 16 L/min.

245 The following elements: Ca, Al, Na, K, Mg, Mn and Fe present in higher concentrations in PM samples,
246 were determined by Inductively Coupled Plasma Atomic Emission Spectroscopy, ICP-AES (Perkin Elmer,
247 model Optima 7000 DV).

248 The power applied was 1300 W. Plasma, auxiliary and nebulizer gas flows were 15, 0.2 and 0.6 L/min
249 respectively. The signals were measured in triplicate.

250 Sets of instrumental blank and calibration verification checks were run at frequent intervals during the batch
251 sequences for both SF-ICP-MS and ICP-AES analyses. The calibrations were performed with standard
252 solutions prepared in aliquots of process blanks. Process blanks were incorporated into the dissolution and
253 analytical procedure to assess metal contribution from the filters, bombs, Milli-Q water and purified acids
254 used in this procedure. Limits of detection (LODs), corresponding to three times the standard deviation of
255 the reagent blank, were experimentally determined by ICP-AES and SF-ICP-MS and are respectively
256 reported in Table 2S and 3S (Supplementary Material).

257 All the elements investigated, namely Al, As, Ba, Ca, Cd, Ce, Co, Cr, Cu, Fe, K, La, Mg, Mn, Mo, Na, Ni,
258 Pb, Sn, Ti, Tl, V, Zn and Zr, are commonly used, with the aid of chemometric treatments and other graphical
259 and mathematical tools, as chemical markers for identifying the anthropogenic and natural (crustal and
260 marine) sources of atmospheric PM.

261 Sampling was carried out over three months, namely May-July 2013, using two distinct types of filters:
262 Millipore® for the first month and Munktell for the remaining time. The sample blank values were
263 measured for each filter type and all the sample signals were subtracted of their appropriate sample blank
264 values. Sample blank concentrations ($\mu\text{g/L}$ or ng/L) are reported in Table 2S and 3S.
265 NIST SRM 1648a (Urban Particulate Matter) and NIES CRM 8 (Vehicle Exhaust Particulates) were used
266 for evaluating the procedural recoveries and for identifying the best analytical parameters. Most of the
267 relative errors for the analytes are lower than 10%, except for some elements of geogenic origin like Al,
268 La, Ce and Ti, which are unlikely to be completely extracted without HF.
269 Finally, the WSI concentrations were determined using an Ion Chromatography (IC) system (Dionex, DX-
270 100, configuration DX 500 for anions and configuration DX 320 for cations). Four circular filter sections
271 (36 mm diameter) for two replicates were placed in 10 mL of HPW and sonicated for 30 minutes to obtain
272 an extraction solution, which was then filtered using a 0.22 μm pore syringe filter. The anion (NO_3^- , Cl^- and
273 SO_4^{2-}) concentrations were measured using an AS11-HC column (4 x 250 mm) with 30 mM KOH while
274 the cation (NH_4^+ , Na^+ , K^+ , Mg^{2+} and Ca^{2+}) concentrations were determined using an Ion Pac CS12A column
275 (4 x 250 mm) with 20 mM methanesulfonic acid as an eluent at a flow rate of 1.0 mL/min. LOD and sample
276 blank concentrations for WSI are reported in Table 4S (Supplementary Material).

277

278 ***2.3 Statistic Data Analysis***

279 The chemometric treatment was carried out using XlStat 2017 software package, an add-on of Microsoft
280 Excel. PCA is a statistical method that uses an orthogonal conversion of a group of observations of possibly
281 correlated variables into a set of uncorrelated variables, obtained by linear combination of the original ones,
282 called principal components (PCs). The number of PCs is less than or equal to the number of original
283 variables. The first principal component has the largest possible variance and the resulting vectors are an
284 uncorrelated orthogonal basis set (Cohen et al., 2003). HCA is a method of group analysis which explores
285 the dataset to build a hierarchy of clusters. An agglomerative procedure was used for clustering: this is a
286 "bottom up" approach, in which each observation starts in its own cluster, and pairs of clusters are merged

287 as one moves up the hierarchy (Rokach and Maimon, 2005). For performing PCA and HCA, the whole
288 dataset was autoscaled. Finally, Kruskal-Wallis test (significance level: 95% and 90%) was performed for
289 checking if the analyte concentrations determined in PM₁₀ samples collected in 2012, 2013 and 2014 in
290 TRM monitoring station were significantly different. The same non-parametric test was used to evaluate if
291 As, Cd, Ni and Pb concentrations in PM₁₀ samples collected in Druento, Torino-Consolata and TRM
292 monitoring stations in 2013 and in May, June and July months in 2014-2018 years were significantly
293 different.

294

295 ***2.3 SRM-Lead isotope ratios analysis***

296 The evaluation of lead isotopic ratios was carried out by SF-ICP-MS considering two circular filter sections
297 of 36 mm of diameter. These sections were punched using an INOX punch: in this way, an enhanced
298 accuracy is guaranteed compared to dividing the filter in four parts using clippers. In fact, the relative
299 standard deviations of replicates were always lower than 10%.

300 In order to evaluate lead isotope ratios, a NIST SRM 981 (Common lead isotopic standard) was used. This
301 certified standard reflects the natural abundance of four lead isotopes: 204 ($1.4255 \pm 0.0012\%$), 206
302 ($24.1442 \pm 0.0057\%$), 207 ($22.0833 \pm 0.0027\%$), 208 ($52.347 \pm 0.0086\%$).

303 SRM 981 was utilized for correcting the bias introduced by instrumental mass discrimination. A solution
304 containing 1.2 mg/L of lead in 0.05% ultrapure nitric acid matrix was prepared for that objective. The values
305 used for the mass bias correction were 0.059042 ± 0.000037 , 0.91464 ± 0.00033 , 2.1681 ± 0.0008
306 respectively for 204/206, 207/206 and 208/206 ratio, as reported on the certificate released by NIST, with
307 errors calculated at 95% confidence interval.

308 A Central Composite Design (CCD) with a total of 27 experiments was chosen to optimize the following
309 instrumental parameters was carried out:

- 310 • Integration window (window of masses to integrate peaks)
- 311 • Sampling points per peak (number of points counted in the window of masses chosen)

312 • Integration times (runs x passes), equal to the replications.
313 The ranges used for these parameters were 60-100%, 5-30 and from 1x1 to 9x9 respectively. These ranges
314 were applied also by Zhu et al. (2006).
315 After evaluating lead concentration in samples analyzed, the concentrations of 2.5 µg/L and 25 µg/L of lead
316 in SRM 981 were chosen, respectively equal to the minimum and the maximum Pb concentration in the
317 samples. In addition, all the measurements were carried out working in both low and medium resolution.
318 In this work, the number of factors (k) is equal to 4 (integration window, sampling points per peak, runs
319 and passes) and 2 levels (L) for each factor were assigned (minimum and maximum value of above reported
320 ranges). Experiments to be realized are equal to $L^k + L * k + n$, where n is the number of the central points
321 (three in this case) (Lundstedt et al., 1998). This chemometric approach was carried out within the software
322 Modde 9.1 (<https://umetrics.com/product/modde>).

323

324 **3. Results and discussion**

325 ***3.1 Chemical composition***

326 ***3.1.1 Mass and element concentrations***

327 The PM₁₀ and element concentrations (mean, standard deviation, and 5th - 95th percentiles) for each month
328 (May, June and July) are reported in Table 1 while PM₁₀ and element concentrations (mean and standard
329 deviation) in each PM₁₀ sample are shown in Tables 5S, 6S and 7S (Supplementary Material).

330

331 **Table 1.** Mean and standard deviation (Mean \pm SD), and 5th - 95th percentiles of each element determined in PM₁₀
 332 samples and PM₁₀ massive concentration, divided by month. All values, except for PM₁₀, are expressed in ng/m³. PM₁₀
 333 is expressed in $\mu\text{g}/\text{m}^3$.

Element	May		June		July	
	Mean \pm SD	5 th - 95 th perc.	Mean \pm SD	5 th - 95 th perc.	Mean \pm SD	5 th - 95 th perc.
PM₁₀	9 \pm 5	5 - 17	31 \pm 4	24 - 35	23 \pm 3	20 - 27
Al	155 \pm 63	90 - 228	477 \pm 205	207 - 688	326 \pm 137	171 - 522
As	0.61 \pm 0.05	0.55 - 0.68	0.80 \pm 0.31	0.46 - 1.23	0.41 \pm 0.09	0.30 - 0.54
Ba	6.05 \pm 1.34	4.50 - 7.93	30.0 \pm 25.0	7.05 - 61.6	35.1 \pm 16.7	12.9 - 49.9
Ca	235 \pm 96	140 - 350	575 \pm 208	296 - 808	354 \pm 139	186 - 530
Cd	0.05 \pm 0.04	0.03 - 0.11	0.08 \pm 0.02	0.06 - 0.11	0.08 \pm 0.01	0.06 - 0.09
Ce	0.16 \pm 0.07	0.08 - 0.25	0.46 \pm 0.23	0.14 - 0.73	0.21 \pm 0.15	0.08 - 0.42
Co	0.08 \pm 0.06	0.03 - 0.16	0.28 \pm 0.35	0.06 - 0.81	0.10 \pm 0.04	0.05 - 0.15
Cr	0.67 \pm 0.57	0.07 - 1.26	3.83 \pm 2.43	0.64 - 6.63	3.29 \pm 1.19	1.63 - 4.63
Cu	9.39 \pm 1.58	7.37 - 11.4	18.6 \pm 3.80	12.8 - 22.4	14.3 \pm 3.83	9.73 - 19.8
Fe	288 \pm 66	210 \pm 365	631 \pm 207	347 - 848	440 \pm 161	251 - 675
K	81.9 \pm 39.3	39 - 133	251 \pm 69	157 - 318	187 \pm 52	140 - 266
La	0.10 \pm 0.04	0.06 - 0.16	0.35 \pm 0.15	0.14 - 0.53	0.21 \pm 0.10	0.11 - 0.37
Mg	142 \pm 80	75 - 254	307 \pm 128	137 - 445	204 \pm 89	101 - 328
Mn	6.30 \pm 1.26	5.33 - 8.25	24.4 \pm 8.7	12.6 - 33.8	14.3 \pm 5.4	8.51 - 21.1
Mo	0.32 \pm 0.11	0.19 - 0.46	0.82 \pm 0.19	0.55 - 1.02	0.67 \pm 0.17	0.45 - 0.89
Na	302 \pm 365	18 - 775	137 \pm 28	96 - 165	76.6 \pm 34	35 - 117
Ni	1.56 \pm 0.66	0.89 - 2.45	3.86 \pm 0.92	2.63 - 4.89	2.37 \pm 0.74	1.59 - 3.48
Pb	1.17 \pm 0.63	0.60 - 2.11	4.81 \pm 1.58	2.88 - 6.98	3.16 \pm 0.74	2.30 - 4.15
Sn	2.91 \pm 0.80	1.77 - 3.73	5.38 \pm 0.91	4.20 - 6.43	3.96 \pm 0.90	2.79 - 5.20
Ti	5.29 \pm 1.65	3.54 - 7.17	14.5 \pm 6.55	6.13 - 21.7	10.7 \pm 4.10	5.96 - 16.4
Tl	0.004 \pm 0.002	0.002 - 0.007	0.019 \pm 0.005	0.013 - 0.025	0.013 \pm 0.002	0.010 - 0.015
V	0.85 \pm 0.81	0.24 - 2.10	3.14 \pm 0.93	2.04 - 4.24	1.17 \pm 0.37	0.71 - 1.62
Zn	14.5 \pm 5.2	8.60 - 21.3	29.3 \pm 13.5	13.0 - 47.0	24.5 \pm 11.6	11.8 - 37.6
Zr	0.41 \pm 0.13	0.29 - 0.61	0.85 \pm 0.24	0.48 - 1.06	0.51 \pm 0.17	0.30 - 0.76

334

335 Generally, PM₁₀ concentrations are smaller in the month of May compared to June and July, as a
336 consequence of an enhanced presence of winds at the ground resulting in longer ranges of dispersion of
337 particulate matter.

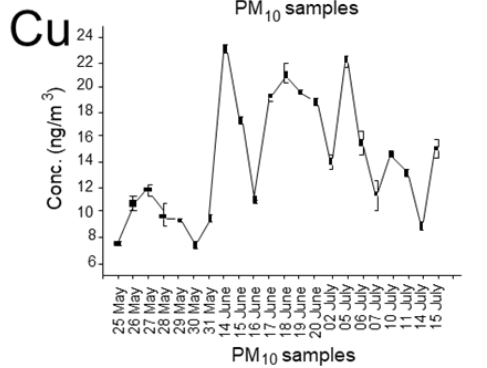
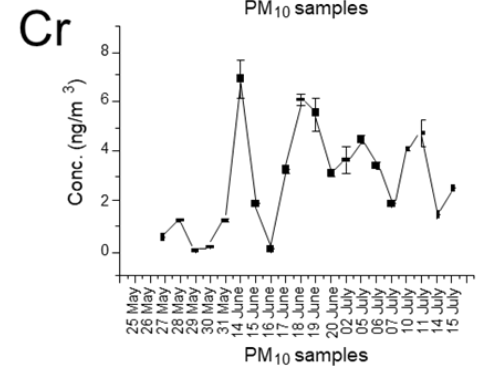
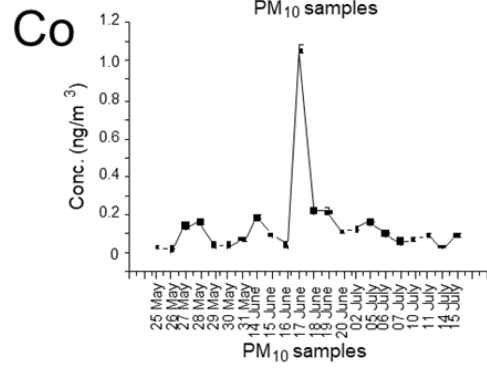
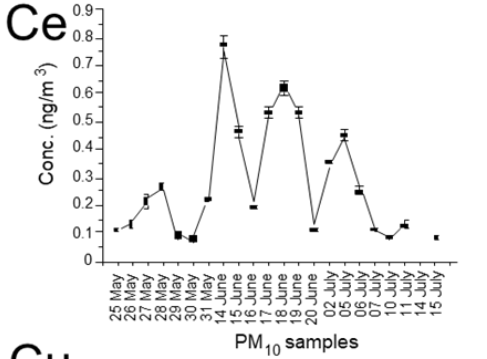
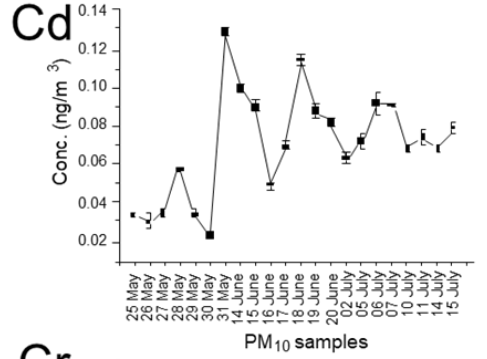
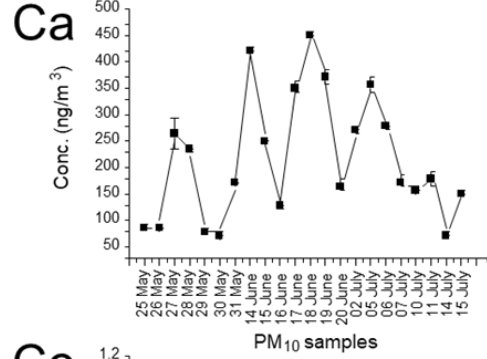
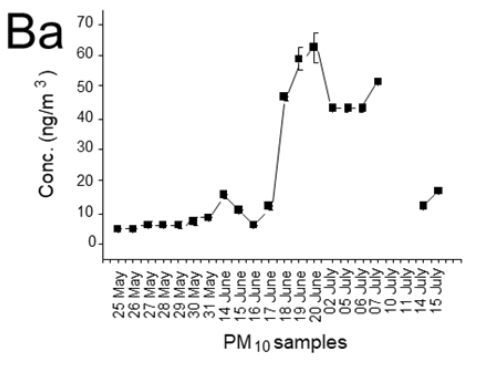
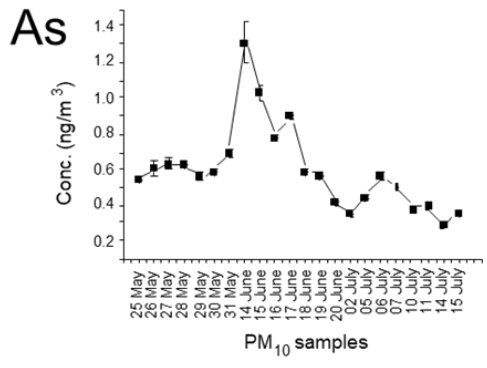
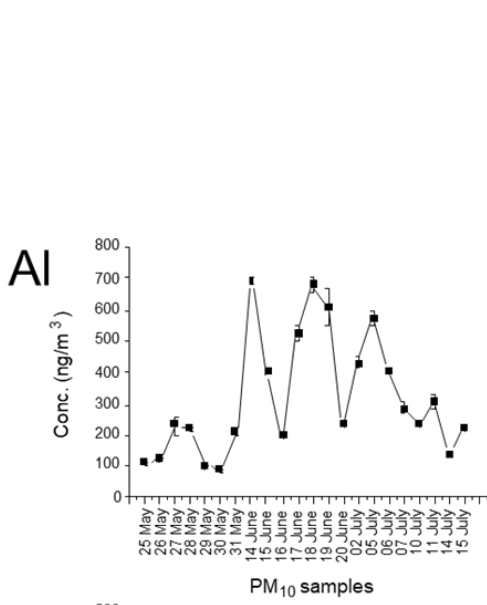
338 Regarding metal concentrations in PM₁₀, the highest concentrations were found for the typically crustal
339 elements, namely for Na, Al, Ca, Fe and Mg, clarifying the significant contribution of soil and re-suspended
340 mineral particles to atmospheric PM, as reported in Padoan et al. (2016).

341 Considering the target values for As, Cd, Ni and the threshold value for Pb, reported in the European
342 legislation (D. Lgs. 155, 2010), that are respectively 6, 5 and 20 ng/m³ for the first three and 0.5 µg/m³ for
343 lead, it is notable that the concentrations of these analytes in all samples are one or two orders of magnitude
344 lower than these values. These elements are the main targets for anthropogenic contributions, especially
345 regarding combustion of fossil fuels and motor vehicles.

346 For trying to evaluate if the start-up phase of the incinerator resulted in an increase of the element
347 concentrations in PM₁₀, the element concentration trends have been considered (Figure 2). Overall, on the
348 basis of the concentration trends, elements could be divided into three groups. Group 1 elements (As, Co,
349 Na and V) show higher concentrations in May and June; Group 2 elements (Al, Ba, Ca, Ce, Cu, Fe, La,
350 Mn, Ni, Ti, Zn and Zr) show an increase in their concentrations in June and at the beginning of July followed
351 by a decrease around the middle of July; the concentrations of Group 3 elements (Cd, Cr, K, Mo, Pb, Sn
352 and Tl) increase between May and June and remain almost constant in July.

353 As and V, belonging to the Group 1, are often referred to be emitted by incinerator plants (Sakata et al.,
354 2000; Font et al., 2015), Na, instead, might derive from NaHCO₃, used at the Turin incinerator plant for the
355 abatement of acids from vapor emissions (<http://trm.to.it/>), the Co behavior is more difficult to explain
356 because it is characterized by a very high concentration in 17 June sample but, to our knowledge, no
357 particular event relating to the incinerator or, in general, to the air quality occurred on that date. It is
358 noteworthy that from 22 May to 5 June the second combustion line was also put into operation for the first
359 time and this could have led to the release of higher concentrations of Na and, to a lesser degree, As and V
360 into the atmosphere.

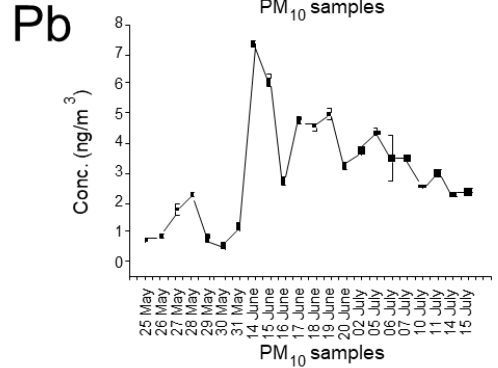
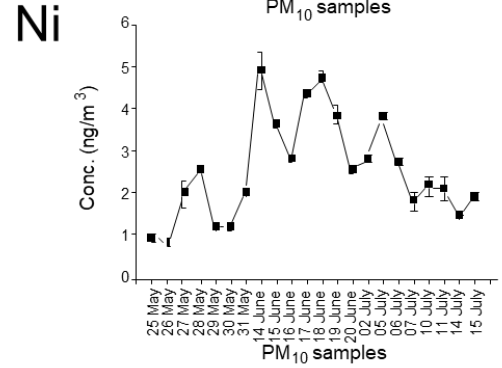
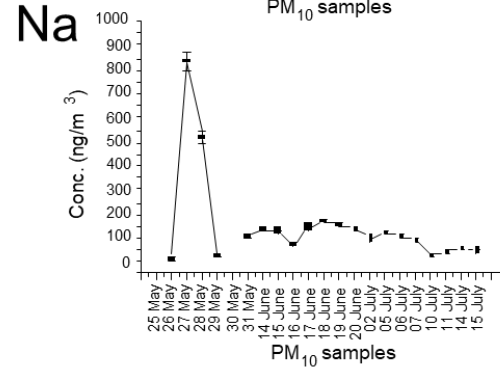
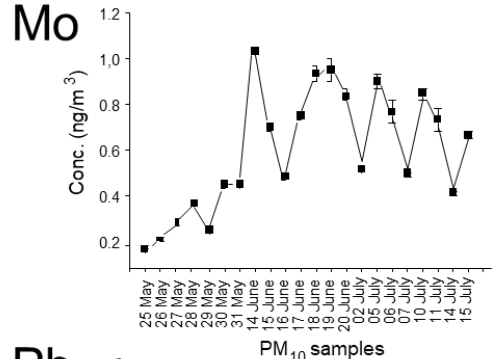
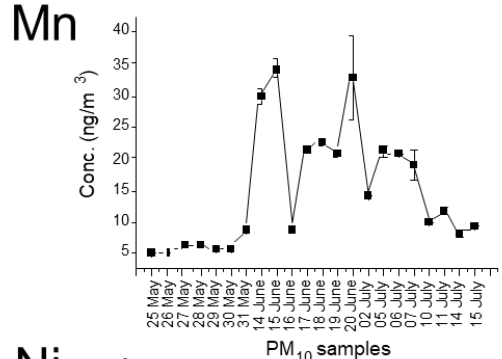
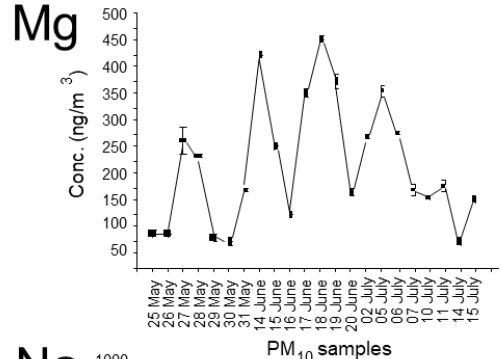
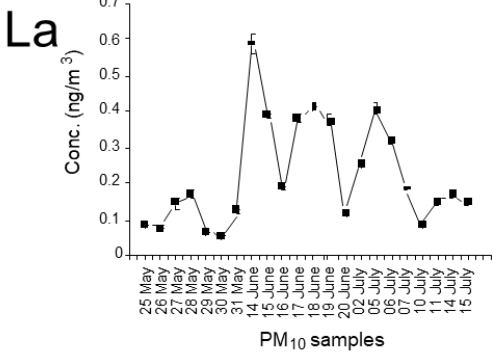
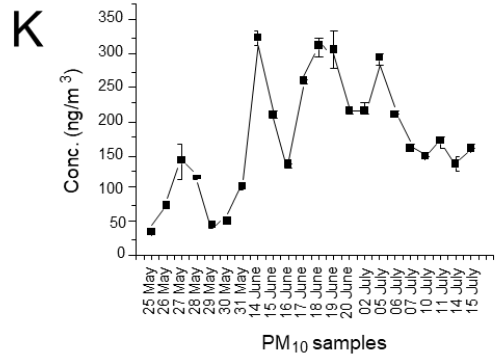
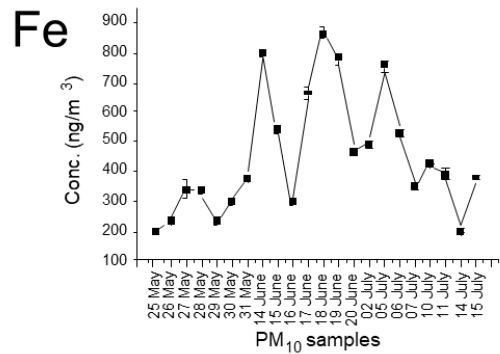
361 Most of the elements belonging to the Group 2 are typically geogenic, precisely Al, Ca, Ce, La, Ti and Zr.
362 The same trend is also shown by Ba, Cu, Fe, Mn and Zn commonly associated also with non-exhaust vehicle
363 emissions, as they are common indicators of release by mechanical abrasion of metal structures of vehicles,
364 engine components, brake and tires wear and road dust (Birmili et al., 2006; Councell et al., 2004; Amato,
365 2008). It is possible that between June and July, due to the start of the incinerator activities and the drier
366 summer climate, proved also by the increase in temperatures recorded starting from mid-June, the road and
367 soil dust resuspension phenomena are intensified, leading to enrichment of the typical elements of these
368 sources in the PM₁₀. Finally, the elements included in Group 3 are typically emitted during several
369 combustion and industrial production processes: in particular Cd, Cr, Pb and Sn are also commonly
370 associated with incinerator emissions (Pacyna et al.,2007; Font et al.,2015).

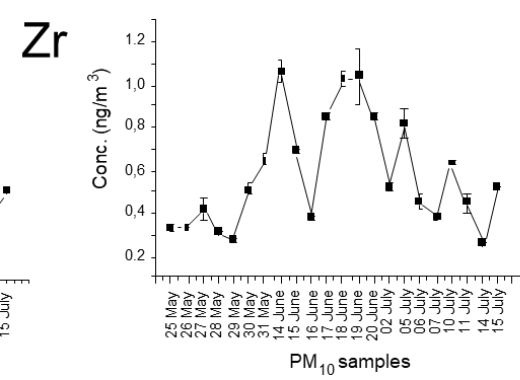
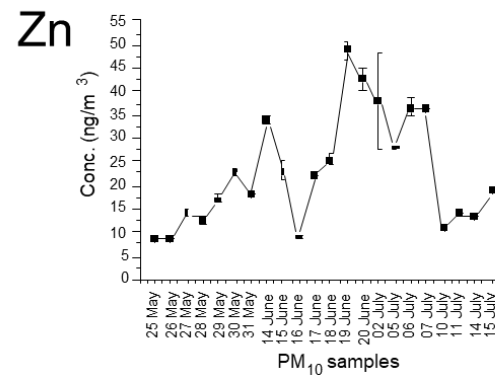
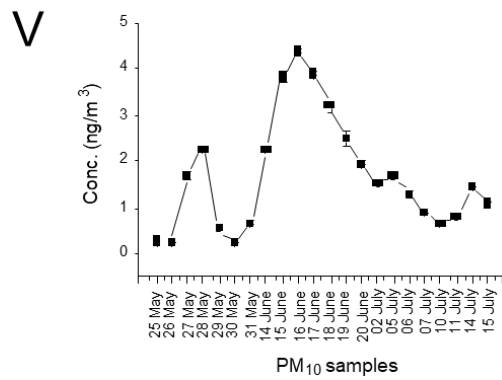
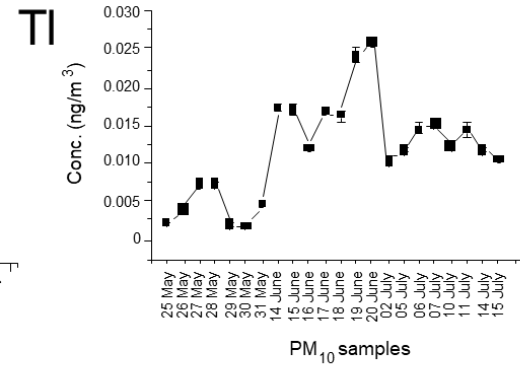
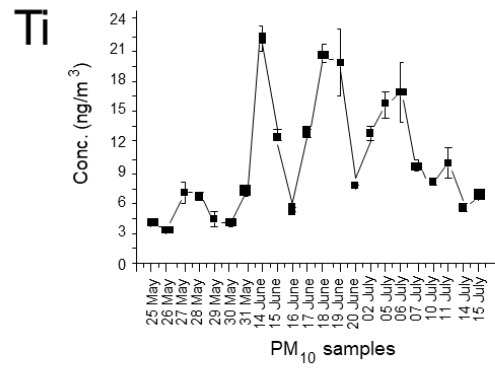
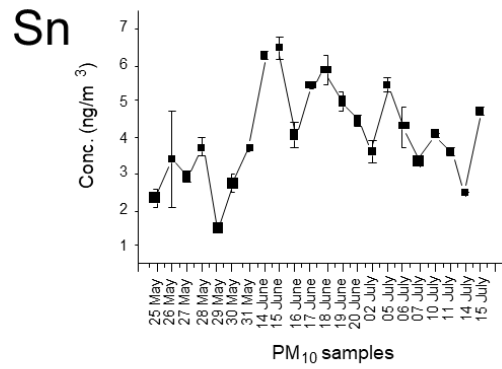


371

372

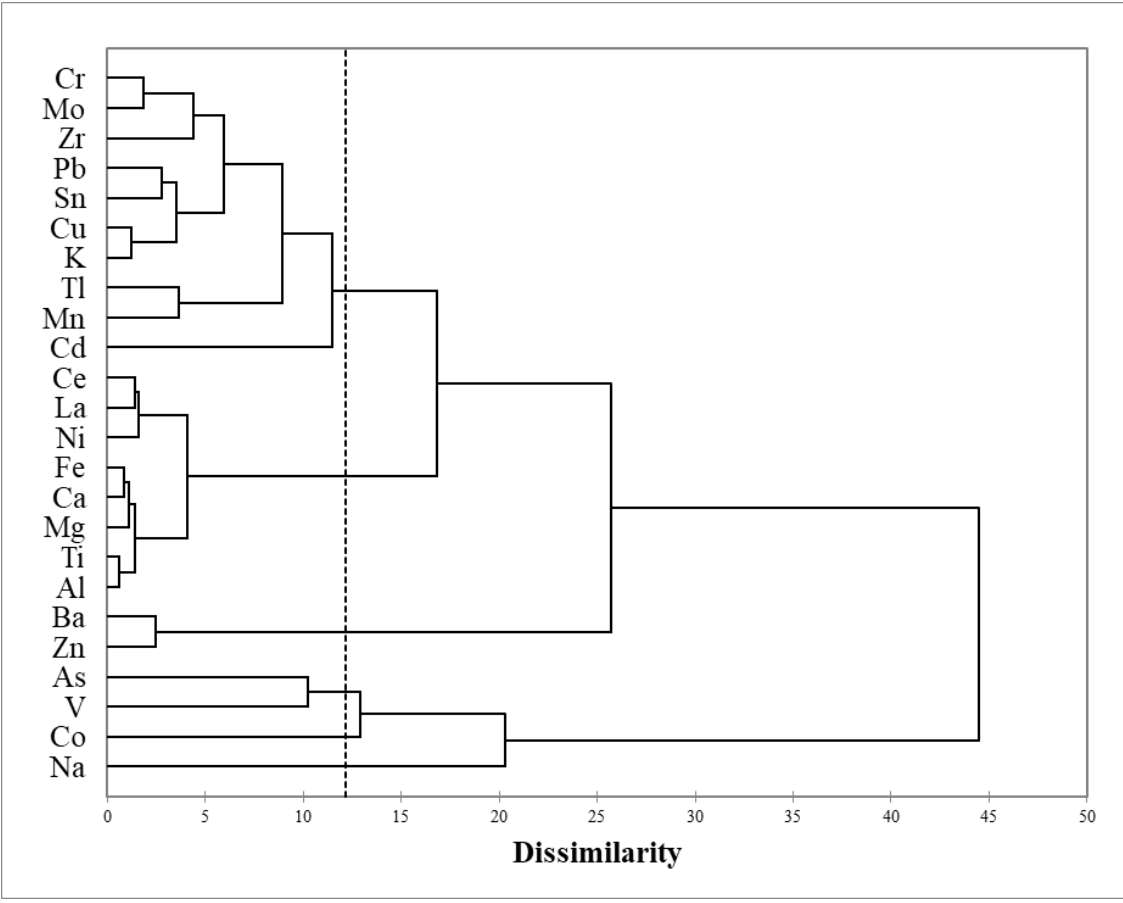
(continued)





376 *Figure 2: Element trends during start-up phase of the incinerator.*

377 In an effort to gain insight into the possible sources of PM₁₀, a chemometric treatment of the experimental
 378 data was carried out through the well-known Q-mode HCA in which we assume that different levels of
 379 dissimilarity among elements are indicative of different emission sources (Figure 3).
 380



381
 382 *Figure 3: Dendrogram obtained by Q-mode HCA*

383
 384 Starting from the bottom of the figure, the first cluster is composed by As, Co, Na and V, i.e. the elements
 385 belonging to Group 1: they are linked at high levels of dissimilarity, suggesting that they do not derive from
 386 a single emission source but they are likely all emitted in atmosphere from several anthropogenic sources,
 387 probably attributable also to activities that have occurred in the start-up phase of the incinerator, such as
 388 the temporary commissioning of the second combustion line. A second cluster is characterized by only two
 389 elements, namely Ba and Zn; several researchers (Pakkanen et al., 2001; Malandrino et al. 2013; Zhang et

390 al. 2020) identified these elements as typical markers of road dust source because the former is added to
391 lubricating oils to prevent smoke and diesel engine abrasion and the latter is also generated by dust caused
392 by vehicular movement or exhaust emission. It is necessary to specify that generally these elements are also
393 associated with crustal elements in identifying the road dust source, while here they are linked at high level
394 of dissimilarity with these elements grouped together in a third cluster. This could be due to the fact that
395 while crustal elements are enriched when the environmental conditions are favorable to the resuspension
396 of soil dust, the resuspension of road dust occurred due to the heavier traffic of trucks carrying the wastes
397 to the incinerator. As already mentioned, the third cluster is characterized by several elements, namely Al,
398 Ca, Ce, Fe, La, Mg, Ni and Ti, that are linked at low levels of dissimilarity, suggesting a common source
399 associated with soil dust. Finally the last cluster groups many elements, namely K, Cr, Cu, Mn, Mo, Pb, Sn,
400 Tl and Zr, that are linked at different levels of dissimilarity, suggesting that they are emitted in atmosphere
401 from several anthropogenic sources. In particular, the clustering of K, Cu, Pb and Sn could represent the
402 direct incinerator emissions since Pb, Sn and Cu are commonly associated with this source and K is a
403 common marker of biomass burning events (Lucarelli et al., 2019) while the other elements probably derive
404 from city vehicular traffic and other industrial activities.

405 Overall, it is likely that the increase of concentrations for Ba, Cd, Cr, Cu, K, Mo, Pb, Sn and Zn during
406 start-up phase of MSWI plant was caused by a combination of factors: the vehicular traffic, presumably
407 increased in this area due to the commissioning of the incinerator, and a possible direct contribution deriving
408 from the incinerator emissions; however, a contribution from the city vehicular traffic and industrial
409 activities cannot be excluded.

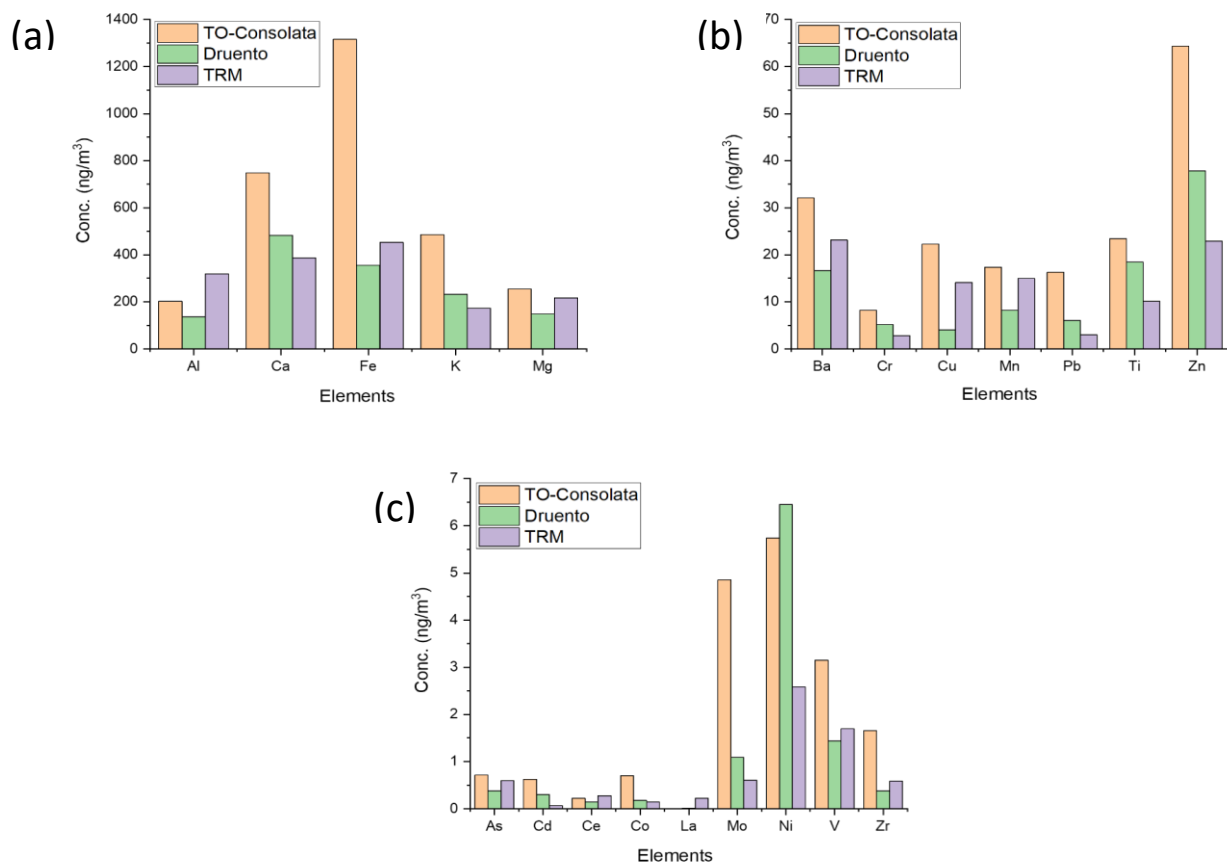
410 In this study, a comparison between results obtained in two nearby areas (Padoan et al., 2016) for an urban
411 site (Torino-Consolata, TO-Consolata) and a rural site (Druento) in 2011 and in the same monitoring station
412 between October and December in 2012 and 2014 was accomplished in order to identify a possible variation
413 of PM sources and/or of their influence due to the MSWI start-up (Table 2). TO-Consolata site is localized
414 in the historical centre of Turin and is mainly affected by vehicular traffic and heating emissions. Druento
415 site is classified as a rural site by ARPA Piedmont and is localized in the small town of Druento, within a

416 regional park, with no direct influence of urban activities. This station is considered as a background site.
417 In Figure 4 it is possible to notice the difference between the three sites for twenty-one elements having
418 high (a), intermediate (b) and low (c) concentrations.

419 **Table 2.** Mean and standard deviation (Mean \pm SD), and 5th - 95th percentiles of each element determined in PM₁₀ samples collected in TRM site in 2013.
 420 For comparison, descriptive statistics of the inorganic composition of the PM₁₀ collected in TRM site in 2012 and 2014 (Conca et al., 2020) and in TO-
 421 Consolata and Druento sites in 2011 (Padoan et al., 2016) are also reported. All the concentrations are expressed in ng/m³.

	This study		2012 TRM		2014 TRM		2011 TO - Consolata		2011 Druento	
	Mean \pm SD	5 th - 95 th perc.	Mean	5 th - 95 th perc.	Mean	5 th - 95 th perc.	Mean	Range	Mean	Range
Al	319 \pm 192	102 – 677	170	33 - 470	250	98 - 530	203	17.8 - 428	137	4.08 - 531
As	0.60 \pm 0.24	0.35 – 1.02	0.48	0.059 - 1.7	1.1	0.26 - 2.9	0.71	0.18 - 1.48	0.38	0.14 – 0.7
Ba	23 \pm 21	4.8 – 58.8	48	19 - 150	52	40 - 78	32.1	12.4 – 76.9	16.7	7.39 – 54.5
Ca	387 \pm 203	139 – 780	580	140 - 1200	1700	840 - 5000	749	18.7 – 1517	482	146 – 1460
Cd	0.07 \pm 0.03	0.03 – 0.11	0.32	0.12 - 0.83	0.29	0.020 - 2.7	0.62	0.19 - 1.08	0.31	0.05 – 1.01
Ce	0.28 \pm 0.21	0.08 – 0.62	0.33	0.076 - 0.66	0.34	0.16 - 0.65	0.22	0 - 0.88	0.15	0 – 1.53
Co	0.15 \pm 0.21	0.036 – 0.22	0.32	0.036 - 1.1	0.31	0.082 - 0.64	0.7	0.06 - 1.85	0.18	0 – 0.87
Cr	2.8 \pm 2.0	0.09 – 6.08	6.4	2.4 - 12	5.2	2.3 - 12	8.24	1.9 – 14.3	5.22	0.51 – 12.5
Cu	14.1 \pm 4.9	7.55 – 22.0	40	7.8 - 79	27	11 - 77	22.3	5.04 – 52.4	3.9	0 – 15.1
Fe	453 \pm 204	203 – 800	1200	260 - 2200	720	230 - 1700	1316	272 - 3164	356	57.4 – 658
K	174 \pm 87	46 – 309	360	61 - 1100	860	330 - 2100	486	79.4 - 1285	232	56.8 – 472
La	0.22 \pm 0.14	0.065 – 0.41	0.19	0.076 - 0.34	0.12	0.060 - 0.34	< 0.007	< 0.007	0.02	0 – 0.47
Mg	217 \pm 117	74 – 421	190	44 - 460	290	170 - 600	254	19 - 738	148	6.77 – 314
Mn	15 \pm 9	5.4 – 33	14	2.6 - 27	12	3.3 - 30	17.3	3.63 – 37.5	8.23	2.04 – 31.3
Mo	0.61 \pm 0.26	0.22 – 0.96	3.4	1.6 - 7.3	3.4	1.1 - 7.3	4.86	0.83 – 16.02	1.09	0.24 – 3.03
Na	154 \pm 192	27 – 538	136	29 – 360	758	172 – 2303	n.a.	n.a.	n.a.	n.a.
Ni	2.6 \pm 1.2	0.96 – 4.8	4.1	0.58 - 9.3	7.7	2.9 - 25.3	5.74	0 – 16.2	6.45	0 – 41.9
Pb	3.0 \pm 1.8	0.76 – 6.0	8.5	0 - 26	10	3.2 - 25	16.3	3.8 – 44.6	6.06	1.7 – 13.2
Ti	10 \pm 6	4.0 – 20	19	1.9 - 51	16	5.0 - 34	23.5	2.29 – 54	18.5	4.99 – 33.7
V	1.7 \pm 1.2	0.26 – 3.9	1.3	0.20 - 3.1	1.2	0.34 - 2.2	3.15	1.06 - 5.73	1.44	0.67 – 2.5
Zn	23 \pm 12	8.7 – 42	68	19 - 160	130	45 - 390	64.3	19.6 - 164	37.9	4.81 – 79.3
Zr	0.58 \pm 0.26	0.28 – 1.04	n.a.	n.a.	n.a.	n.a.	1.66	0.29 – 4.01	0.38	0 – 3.43

422 n.a.: not available



424 **Figure 4:** Concentrations of metals and metalloids in PM_{10} in TO-Consolata (urban), Druento (rural)
 425 and TRM (sub-urban) sites. (a) high, (b) intermediate and (c) low concentrations.

426

427 Generally, the concentration of analytes in TRM site is in between with respect to the urban site and the
 428 rural one. In the urban site higher concentrations of analytes deriving from anthropogenic activities were
 429 measured, due to vehicular traffic and industrial and residential combustion processes.

430 On the other hand, Al, La and Ce concentrations are slightly higher in the TRM site than in the other two
 431 locations. Since the most probable common source for these elements is represented by the Earth's crust,
 432 their concentration is usually higher when soil dust resuspension events are more likely, that is when higher
 433 speed of wind is observed, as reported in May month in TRM site.

434 TRM site is considered a sub-urban site. Indeed, concentrations of these target metals are quite high

435 compared to rural sites, but still they are comparable to other sub-urbans sites (Gholampour et al., 2016).
436 Finally, the element concentrations in TRM site during start-up phase of the incinerator are comparable or
437 lower than those found in PM₁₀ samples collected in the same monitoring station in 2012 and 2013. This
438 mainly happens due to the frequent thermal inversions occurring during autumn and winter. These climatic
439 phenomena have a relevant effect, particularly in orographically complex areas such as the Alpine arc
440 surrounding the North-West sector of Piedmont. The stagnation of air in the valley floors, caused by severe
441 thermal inversions in winter, gives rise to an accumulation of all pollutants. In some situations, when the
442 thermal inversion is very strong while the foehn winds are weak, air recirculation is limited, resulting in
443 intense urban pollution. These results underline the unquestionable role of meteorology in the evolution of
444 pollutant concentrations in air and the overall low contribution of elements arising from MSWI plant also
445 during the start-up phase.

446 Finally, in Table 3, we compare the total PM₁₀, As, Cd, Ni and Pb concentrations found in PM₁₀ samples
447 collected in Torino Consolata, Druento and TRM sites in all 2013 and in May – July quarters of 2014-2018.
448 It is evident that the concentrations for these elements in TRM site are in between the other two sites (ARPA
449 Piemonte, 2013a; ARPA Piemonte, 2013b; ARPA Piemonte, 2014; ARPA Piemonte, 2015; ARPA
450 Piemonte, 2016; ARPA Piemonte, 2017; ARPA Piemonte, 2018).

451

452 **Table 3.** Concentrations (mean \pm standard deviation; min-max) of total PM₁₀ (expressed in $\mu\text{g}/\text{m}^3$) as well as As, Cd,
 453 Ni and Pb (expressed in ng/m^3) in 2013 and in May – July quarters of 2014-2018 for TO-Consolata (urban), Druento
 454 (rural) e TRM (sub-urban) sites.

Element	2013			2014-2018 (May-July)		
	TO-Consolata	Druento	TRM	TO-Consolata	Druento	TRM
PM ₁₀	40 \pm 28	24 \pm 16	33 \pm 23	21 \pm 7	18 \pm 3	18 \pm 7
	(5 – 144)	(5 – 101)	(4 – 110)	(5 – 46)	(5 – 71)	(4 – 45)
As	0.71 \pm 0.03	0.71 \pm 0.03	0.71 \pm 0.03	0.7	0.7	0.7
	(0.7 – 0.8)	(0.7 – 0.8)	(0.7 – 0.8)	(0.7 – 0.7)	(0.7 – 0.7)	(0.7 – 0.7)
Cd	0.23 \pm 0.34	0.12 \pm 0.04	0.22 \pm 0.16	0.1	0.1	0.1
	(0.1 – 1.2)	(0.1 – 0.2)	(0.1 – 0.6)	(0.1 – 0.1)	(0.1 – 0.1)	(0.1 – 0.1)
Ni	4.88 \pm 2.50	1.59 \pm 1.14	2.95 \pm 1.63	2.7 \pm 1.3	3.0 \pm 5.4	2.3 \pm 1.2
	(2 – 11)	(0.7 – 3.8)	(0.7 – 5.8)	(0.7 – 5.4)	(0.7 – 23)	(0.7 – 5.3)
Pb	10 \pm 6	4.2 \pm 2.5	8.9 \pm 5.6	4.2 \pm 0.8	2.1 \pm 0.8	3.1 \pm 1.3
	(4 – 26)	(1 – 9)	(2 – 21)	(3 – 6)	(1 – 4)	(1 – 6)

455

456 No significant differences can be evidenced by Kruskal-Wallis test (significance level: 95%) due to the
 457 high variability of As, Cd, Ni and Pb concentrations in PM₁₀ samples, but it is however possible to make
 458 some general considerations. More precisely, relative to the whole year 2013, arsenic concentrations are
 459 similar in the three sites, while PM, cadmium and lead concentrations are higher in TO-Consolata site where
 460 the traffic and combustion phenomena are prevalent. Ni concentrations in the urban site are approximately
 461 thrice and twice higher than in the rural and sub-urban sites respectively. Considering, instead, the May-
 462 July quarters in the 2014-2018 period, it is evident that Cd and As concentrations are similar in the three
 463 sites, while Ni and Pb concentrations are lower in TRM site than in TO-Consolata site. Finally, relative to
 464 Druento, the Pb concentrations are higher and Ni concentrations are lower in TRM site. The anomalous Ni

465 behavior can be explained taking into account that the Druento site is located in a large regional park and,
466 therefore, in spring-summer it is more subject to episodes of soil dust resuspension that increase Ni
467 concentrations in PM, due to the high background levels of this element in Piedmont soils (Biasioli et al.,
468 2006; Bonifacio et al., 2010; Padoan et al., 2016); this is also confirmed by high variability of Ni
469 concentrations in this site. The Pb behavior, instead, is a further confirmation of its possible anthropogenic
470 input to the PM in TRM site. However, since Pb is one of the principal markers of incinerator emission, a
471 further study of lead isotopic ratios was performed in order to identify the possible sources of lead in the
472 airborne particulate matter collected in TRM site.

473 In addition, we compared our results with target metals found in PM₁₀ emitted from Municipal Solid Waste
474 Incinerators (MSWI) located in UK (Font et al., 2015), where As, Cd, Cr, Cu, Pb, Mn, Ni and V were
475 considered as target pollutants of MSWI emissions. In all cases, considering maximum values, the element
476 concentrations near such plants are several orders of magnitude higher than in TRM site (e.g., Pb
477 concentration is 7.35 ng/m³ in this study and 200 µg/m³ in MSWI sites in UK (Font et al., 2015). This
478 demonstrates that incinerators of new installation have a lower impact on atmospheric particulate matter
479 composition thanks to current legislation and up-to-date technologies.

480 Moreover, to evaluate if the incinerator installed near Turin city influenced the PM₁₀ composition, Cu/Pb,
481 Cd/Cu, Cr/Pb, and Cd/Pb ratios were calculated and compared with the values reported for MSWI, rural
482 and traffic emissions in Font et al. (2015). These ratios were used to discriminate between the different
483 sources of potentially toxic metals in airborne particulate matter. Table 4 shows that average values of
484 Cu/Pb, Cd/Cu and Cd/Pb calculated in this study are prevalently typical of traffic pollution. Therefore, we
485 can assume that the major contribution in Cu, Pb and Cd to PM₁₀ collected in TRM site is due to the traffic
486 instead of being originated from the emissions of the incinerator. The high value found for Cr/Pb ratio is
487 probably due to a relevant natural contribution for chromium from soils: as reported above, Piedmont plains
488 originated during past fluvio-glacial events and are therefore made of sediments, which partly derive from
489 serpentinitic areas; this, as already documented by other researchers (Biasioli et al., 2006; Bonifacio et al.,
490 2010; Padoan et al., 2016), causes high background levels of Ni and Cr in soils and in soil dust.

491

492 **Table 4.** Typical Cu/Pb, Cd/Cu, Cr/Pb and Cd/Pb ratios calculated in this study compared with rural situation, MWI
493 and traffic pollution (Font et al., 2015).

Ratio	This study	MSWI	Rural	Traffic
Cu/Pb	4.62	0.83	0.51	2.38
Cd/Cu	0.005	0.14	0.026	0.007
Cr/Pb	0.81	0.56	0.13	0.28
Cd/Pb	0.023	0.08	0.013	0.017

494

495 Finally, Enrichment Factors (EFs) were calculated with respect to the mean values for the Earth’s upper
496 crust reported by Wedepohl (1995), in order to distinguish elements having geologic or non-geologic origin.

497 The equation used is the following:

498
$$EF_i = \frac{C_{i PM} / C_{r PM}}{C_{i crust} / C_{r crust}}$$

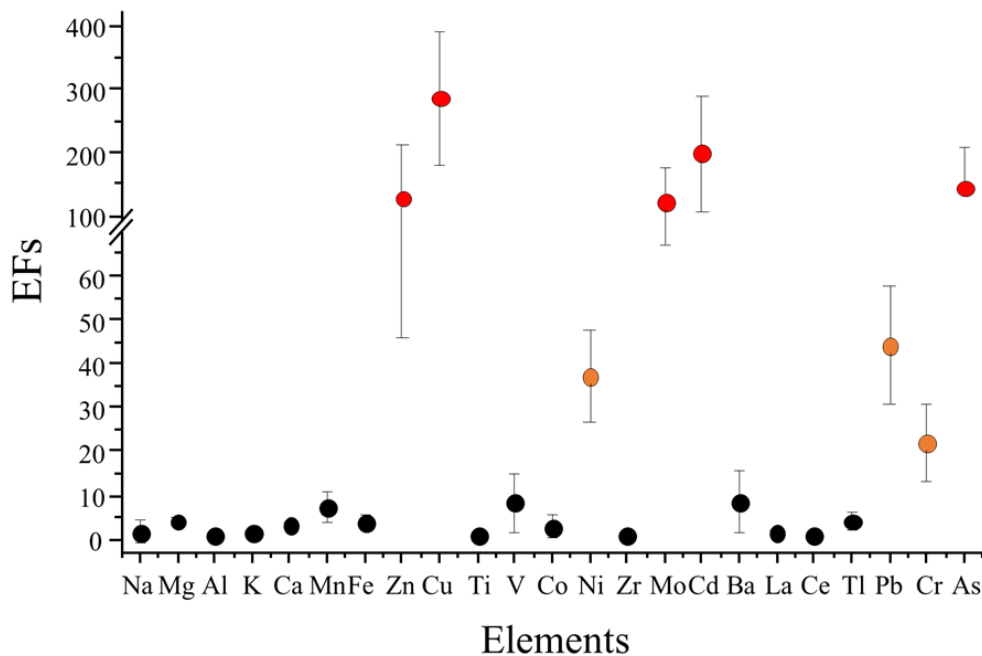
499 where $C_{i PM} / C_{r PM}$ and $C_{i crust} / C_{r crust}$ are the ratios between the concentration of the element i and the
500 concentration of a reference element r respectively in the sample and in the upper crust; in this work, Al
501 was selected as a reference element. By convention, EFs lower than 10 are taken as an indication that an
502 element has a prevailing geogenic origin, EFs between 10 and 100 indicate a moderate enrichment and EFs
503 higher than 100 indicate that the element (called “enriched”) has a prevailing non-geogenic origin (Lai et
504 al., 2017; Tahri et al., 2017).

505 The average values of EFs were reported in Figure 5.

506

507

508



509

510 **Figure 5.** Enrichment Factors for elements determined in PM₁₀ samples.

511

512 As, Cd, Cr, Cu, Mo, Ni, Pb and Zn are predominantly generated by anthropic activities, with EFs values
 513 higher than 10. These EFs are not higher than those reported for the city of Turin in previous studies (Padoan
 514 et al., 2016), which represents a further confirmation that the installation of MSWI plant did not lead to an
 515 increase in polluting emissions into the atmosphere. Finally, the elements moderately or highly enriched in
 516 this sampling station can arise from vehicle emissions which likely increased in this area due to the opening
 517 of the MSWI plant.

518

519 *3.1.2 Water-soluble ions concentrations*

520 The concentrations of major WSI and their contribution to the PM₁₀ concentrations are shown in Table 5,
 521 where it can be seen that the respective average concentrations of the total WSI were 2.93, 8.87 and 5.16
 522 µg/m³ for May, June and July and accounted for 33.06%, 28.89% and 22.67% of the PM₁₀ mass. The average
 523 percentage was equal to 28.21%, a percentage slightly lower compared to other studies (Ochsenkühn et al.,

524 2008; Li et al., 2015) where WSI is equivalent to 40%, but higher compared to a different work (Fan et al.,
 525 2014), where WSI of 12% was measured. The concentrations of the WSI were dominated by NO_3^- , SO_4^{2-}
 526 and NH_4^+ , followed by Ca^{2+} , Na^+ , K^+ , Mg^{2+} and Cl^- . It is also shown that secondary inorganic ions (SII:
 527 NO_3^- , SO_4^{2-} and NH_4^+) accounted for 77.37%, 89.13% and 87.98%, respectively, of the WSI for May, June
 528 and July. In Table 5, it can be seen that the mean concentrations of the total WSI were higher in June and
 529 July than in May: this is likely due to more consistent weather conditions in the two summer months.

530

531 **Table 5.** Mean and standard deviation (Mean \pm SD), and 5th - 95th percentiles of major water-soluble ions (WSI),
 532 divided by month. All the concentrations are expressed in ng/m^3 except NH_4^+ , NO_3^- and SO_4^{2-} which are expressed in
 533 $\mu\text{g}/\text{m}^3$.

Element	May		June		July	
	Mean \pm SD	5 th - 95 th perc.	Mean \pm SD	5 th - 95 th perc.	Mean \pm SD	5 th - 95 th perc.
Cl^-	68 \pm 110	19 – 234	20 \pm 1	< 19 - 21	19 \pm 1	< 19 – 21
NO_3^-	1.07 \pm 0.9	0.48 – 2.48	4.8 \pm 0.8	3.63 – 5.43	2.7 \pm 0.5	2.23 – 3.53
SO_4^{2-}	0.90 \pm 0.83	0.27 – 2.11	1.5 \pm 0.5	0.81 – 2.03	0.83 \pm 0.30	0.45 – 1.24
NH_4^+	0.30 \pm 0.23	0.14 – 0.66	1.6 \pm 0.2	1.34 – 1.94	0.99 \pm 0.20	0.79 – 1.28
Ca^{2+}	203 \pm 88	105 – 318	628 \pm 196	351 – 830	411 \pm 164	222 – 629
K^+	77 \pm 22	46 – 103	134 \pm 37	99 – 188	97 \pm 19	78 – 123
Mg^{2+}	41 \pm 43	10 – 107	57 \pm 13	37 – 66	39 \pm 12	23 – 54
Na^+	273 \pm 383	29 – 873	125 \pm 19	103 – 150	55 \pm 16	33 – 73
SII	2266 \pm 1916	922 – 5251	7909 \pm 853	6816 – 9035	4538 \pm 822	3729 – 5844
WSI	2928 \pm 2475	1168 – 6654	8873 \pm 825	7859 – 9981	5158 \pm 883	4295 – 6525

534

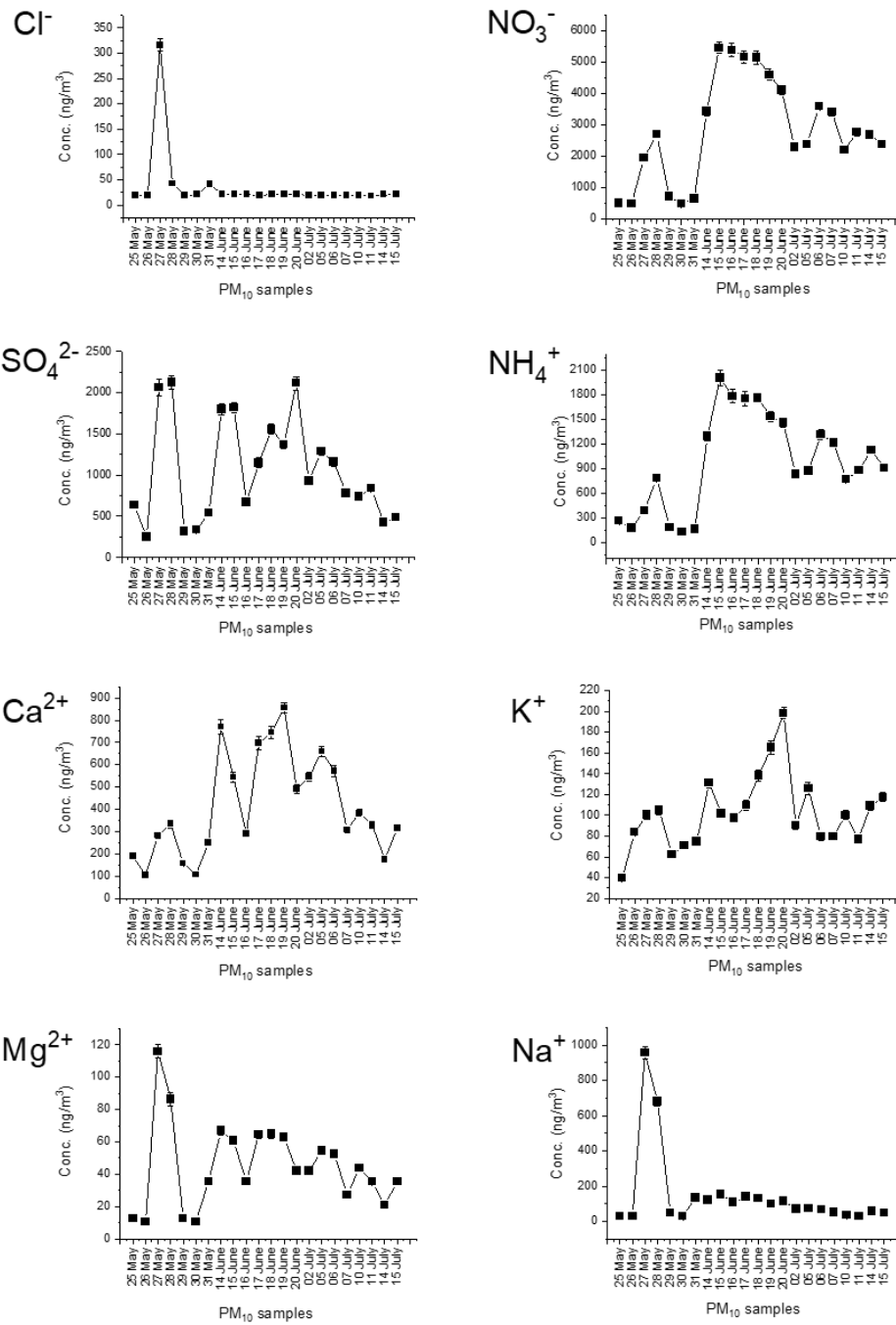
535 More in detail, anions content is larger compared to the cations one (19.70% vs 8.51%), prevalently
 536 attributable to nitrates (13.08%) and sulfates (5.92%) produced by combustion processes in vehicles and
 537 industries respectively. The main component of WSI is overall ammonium nitrate (Pearson's correlation
 538 index between NH_4^+ and NO_3^- is 0.985).

539 It has been reported that the mass ratio of nitrate/sulphate can be used to evaluate the relative contribution
 540 of mobile and stationary sources in the atmosphere (Xu et al., 2012; Zhou et al., 2016). The mass ratios of

541 $\text{NO}_3^-/\text{SO}_4^{2-}$ in May, June and July were 1.19, 3.18 and 3.26 respectively; they were therefore greater than
542 one, and this was especially true in June and July, which indicates that mobile sources (e.g. vehicle exhaust)
543 make a greater contribution to aerosol pollution than stationary sources (e.g. incinerator). It should be noted
544 that the mass ratios of $\text{NO}_3^-/\text{SO}_4^{2-}$ increased greatly in the two summer months, which suggests that the
545 vehicular traffic may have a more important effect on the PM_{10} concentration in the investigated area when
546 the weather conditions are more stable.

547 Finally, higher concentrations of Na^+ and Cl^- were found in May (Figure 6), when also the second
548 combustion line of the incinerator was active. Direct incinerator emissions are conceivable sources for these
549 ions: Na is used such as NaHCO_3 at the Turin incinerator plant for the abatement of acids from vapor
550 emissions (<http://trm.to.it/>) and, hence, it can combine with hydrochloric acid present in gaseous fumes
551 arising from the combustion of organic chlorine present in waste (e.g. plastics, PVC, chlorinated solvents);
552 NaCl can also be already present in the form of salt contained in paper and cardboard, food and vegetable
553 waste. Moreover, it is interesting to note that, in May, when the NaCl concentration is higher, the NH_4NO_3
554 concentration is lower. This represents a further confirmation that NaCl is one of the main sinks of NH_4NO_3
555 in the aerosol (Ochsenkühn et al., 2008).

556



557

558 *Figure 6: Concentration trends during start-up phase of the incinerator for water-soluble ionic*

559 *components.*

560 **3.2 Optimization of instrumental parameters for Pb isotope ratios analysis**

561 The optimization of the experimental conditions of the instrumental parameters for Pb isotope ratios was
562 carried out following the factorial design of experiments and response surface methodology, originally
563 developed by Box and Wilson. In order to reduce the number of measurements we decide to perform a
564 Central Composite Design (CCD) considering four instrumental parameters at the same time. In Table 6
565 are reported the experimental parameters and the investigated ranges. A total of 24 different operative
566 conditions plus 3 central points were considered.

567

568 **Table 6.** Investigated instrumental parameters and their range.

<i>INSTRUMENTAL PARAMETERS</i>	<i>LOW</i>	<i>INTERMEDIATE</i>	<i>HIGH</i>
Integration window (%)	60	80	100
Sampling points per peak	5	17	30
Run	1	5	9
Passes	1	5	9

569

570 Experiments were carried out randomly, both in low and medium resolution, using the two concentrations
571 of SRM 981 standard (2.5 and 25 µg/L). Blank signal was subtracted for all the tests, and the interference
572 of ²⁰⁴Hg was considered with respect to ²⁰⁴Pb by calculating mathematically the amount of this isotope after
573 measuring ²⁰²Hg that is not affected by any spectral interferences.

574 For each experiment the total accuracy was evaluated, that is the average of the absolute value of the
575 accuracies for every isotope, together with the precision, that is the relative standard deviation of the
576 accuracy for all the isotopes. Both accuracy and precision are expressed as percentages. Table 7 reports the
577 results obtained for all the meaningful experiments in low and medium resolution, with the accuracy and
578 the precision at SF-ICP-MS, at both 2.5 µg/L and 25 µg/L concentration of NIST SRM 981.

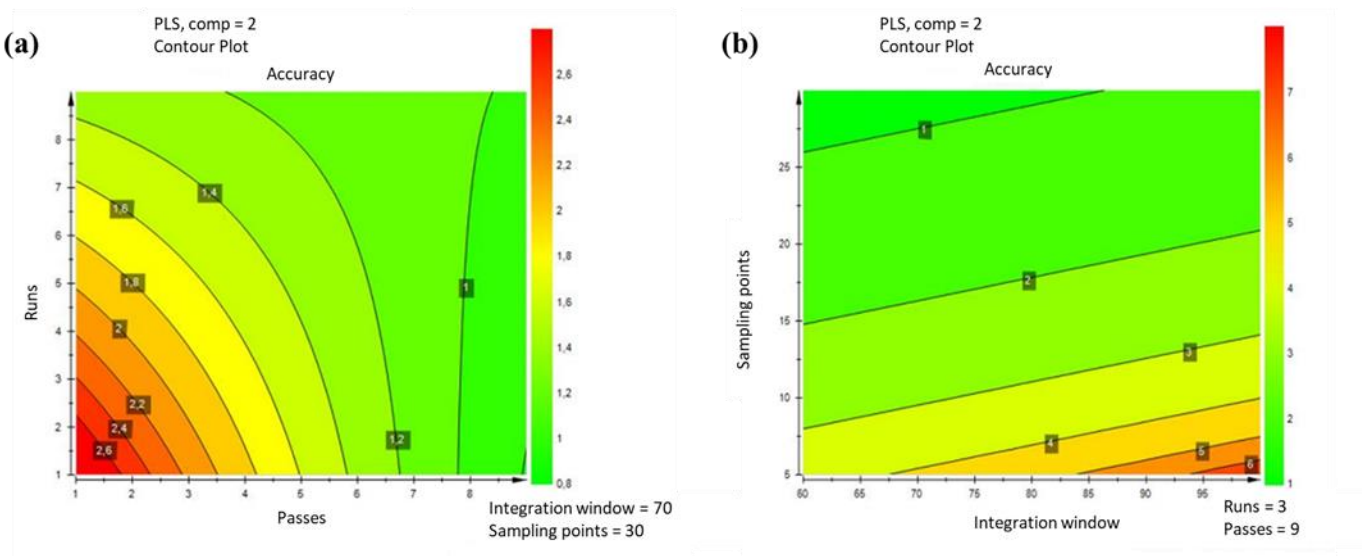
579

580 **Table 7.** Experiments set selected by CCD and carried out in LR (low resolution) and MR (medium resolution) for
 581 the 2.5 and 25 µg/L of SRM981 concentration (results for experiments N2, N10, N13, N14 and N18 are not reported
 582 because of the too low number of sampling points per peak).

Experiment	Accuracy	Precision	Accuracy	Precision	Accuracy	Precision	Accuracy	Precision
	2.5 µg/L	2.5 µg/L	25 µg/L	25 µg/L	2.5 µg/L	2.5 µg/L	25 µg/L	25 µg/L
	LR	LR	LR	LR	MR	MR	MR	MR
N1	2.59	2.05	5.45	6.8	17.35	8.34	11.29	13.05
N3	4.19	2.04	6.53	1.01	7.24	5.21	9.46	1.47
N4	4.77	5.64	2.73	1.77	7.06	6.01	1.2	0.41
N5	2.02	1.91	4.31	1.45	5.89	2.19	2.78	1.92
N6	9.84	11.02	2.28	3.11	8.6	8.93	4.55	0.17
N7	1.53	1.56	1.6	1.75	3.19	3.43	0.74	0.78
N8	1.05	1.2	1.62	1.62	1.66	0.86	3.94	1.33
N9	2.74	0.65	2.93	2.45	2.33	2.96	5.03	5.92
N11	0.83	0.97	1.95	2.01	2.73	3.17	1.32	0.52
N12	1.01	1.33	0.57	0.09	3.56	4.34	3.06	2.89
N15	1.06	1.06	1.05	1.06	0.82	0.98	0.96	0.75
N16	1.52	1.31	1.01	1.1	2.41	1.75	0.92	1.12
N17	1.24	1.14	1.24	1.54	0.94	0.75	0.95	0.73
N18	2.19	2.14	2.6	1.29	3.1	1.36	0.62	0.67
N20	1.46	1.44	0.74	0.84	4.91	2.76	5.77	2.53
N21	4.21	3.34	2.12	1.44	5.7	5.08	4.15	3.71
N22	0.8	0.94	1.97	1.02	3.77	1.7	0.87	0.77
N23	2.65	2.75	2.43	2	4.19	3.71	3.89	2.02
N24	1.63	1.75	1.26	1.49	1.21	1.46	1.05	0.83
N25	2.34	2.43	1.85	0.79	1.05	0.78	1.19	0.84
N26	3.64	1.33	2.77	2.16	1.35	1.7	2.96	0.72
N27	2.64	1.97	0.61	0.58	0.8	0.89	2.43	2.22

583
 584 Four groups of tests (responses) were carried out, for the two concentrations of NIST SRM 981 (2.5 and 25
 585 µg/L) in low and medium resolution. A PLS (Partial Least Square) regression was applied to obtain a
 586 second-order model by projecting the predicted variables and the observable ones to a new space
 587 considering accuracy, precision and the four variables aforementioned. Variables were scaled at unit

588 variance when the model was fitted. The results were used to provide the minimum values of accuracy and
589 precision (expressed in percentages) depicted in green in Figure 7.



590
591 **Figure 7:** The effect of runs and passes (a) and sampling points and integration window (b)
592 of lead isotope ratios determination.

593
594 In this way we were able to identify the experimental conditions with the closer values to the certified one
595 and with minimum dispersion.

596 Among the four variables, sample points per peak was the most important one respect to accuracy and
597 precision. The optimum response was obtained using 2.5 $\mu\text{g/L}$ of SRM 981 concentration in low resolution.

598 The related optimal values of the four variables (3 runs, 9 passes, 70% of integration window and 30
599 sampling points per peak) produced values equal to a $0.83 \pm 0.46\%$ of accuracy and $0.75 \pm 0.42\%$ of

600 precision. Those operative conditions were successfully used in the isotopic investigation of lead for the
601 PM_{10} samples.

602

603 3.3 Lead isotope ratios determination

604 Lead concentration is low in all the samples analyzed, with values between 0.8 ng/m³ (during May) and 7.4
 605 ng/m³ (during June). EFs are in the range between 26.4 and 71.9, indicating a slightly anthropogenic
 606 contribution for Pb in the PM₁₀ samples.

607 Lead isotope ratios for all PM₁₀ samples (Tables 8 and 8S) were determined, by adopting the optimized
 608 experimental conditions previously described (paragraph 3.3), in order to identify more accurately the
 609 possible sources of this element in the investigated area.

610

611 **Table 8.** Mean and standard deviation (Mean ± SD), median, and 5th - 95th percentiles of the lead isotope ratios
 612 (namely ²⁰⁴Pb/²⁰⁶Pb, ²⁰⁶Pb/²⁰⁷Pb and ²⁰⁸Pb/²⁰⁶Pb ratios) according to the month.

²⁰⁴ Pb/ ²⁰⁶ Pb	May	June	July
Mean ± SD	0.0532 ± 0.0008	0.0545 ± 0.0021	0.0514 ± 0.0013
Median	0.0532	0.0551	0.0508
5 th - 95 th perc.	0.0519 – 0.0540	0.0515 – 0.0566	0.0502 – 0.0533
²⁰⁶ Pb/ ²⁰⁷ Pb	May	June	July
Mean ± SD	1.1595 ± 0.0066	1.1578 ± 0.0166	1.1766 ± 0.0325
Median	1.1601	1.1643	1.1908
5 th - 95 th perc.	1.1502 – 1.1670	1.1327 – 1.1711	1.1351 – 1.2102
²⁰⁸ Pb/ ²⁰⁶ Pb	May	June	July
Mean ± SD	2.0347 ± 0.124	1.9952 ± 0.0581	1.9300 ± 0.0550
Median	2.0922	2.0176	1.9106
5 th - 95 th perc.	1.8507 – 2.1216	1.9059 – 2.0473	1.8806 – 2.0143

613

614 With a view to monitor accuracy together with precision of measurements, periodical readings of SRM 981
 615 were performed.

616 With the aim to define which are the sources of lead in the PM₁₀ samples, the isotopic signature of each
617 possible source for Pb should be known. This signature is a consequence of the mineral characteristic of
618 the soil or of the material from which industrial lead was extracted. Generally, it was observed that
619 atmospheric Pb was mainly influenced by traffic during the first part of Nineties of the twentieth century,
620 followed by a mixed influence on traffic and industry during the 1995-1999 period. After 2000, when leaded
621 gasoline was forbidden in Europe, the greatest part of atmospheric lead is coming from industrial activities
622 (De la Cruz et al., 2009; Widory et al., 2004).

623 While each lead source has its own specific isotopic composition, it is useful to note that separate
624 geochemical reservoirs are linked together and the final isotopic composition of lead results from mixing
625 of many diverse sources.

626 Tropospheric lead, when is produced by anthropic activities, is mostly associated with the submicrometric
627 aerosols that can be transported over long distances making thus the interpretation of lead isotopic data not
628 easy (Flament et al., 2002).

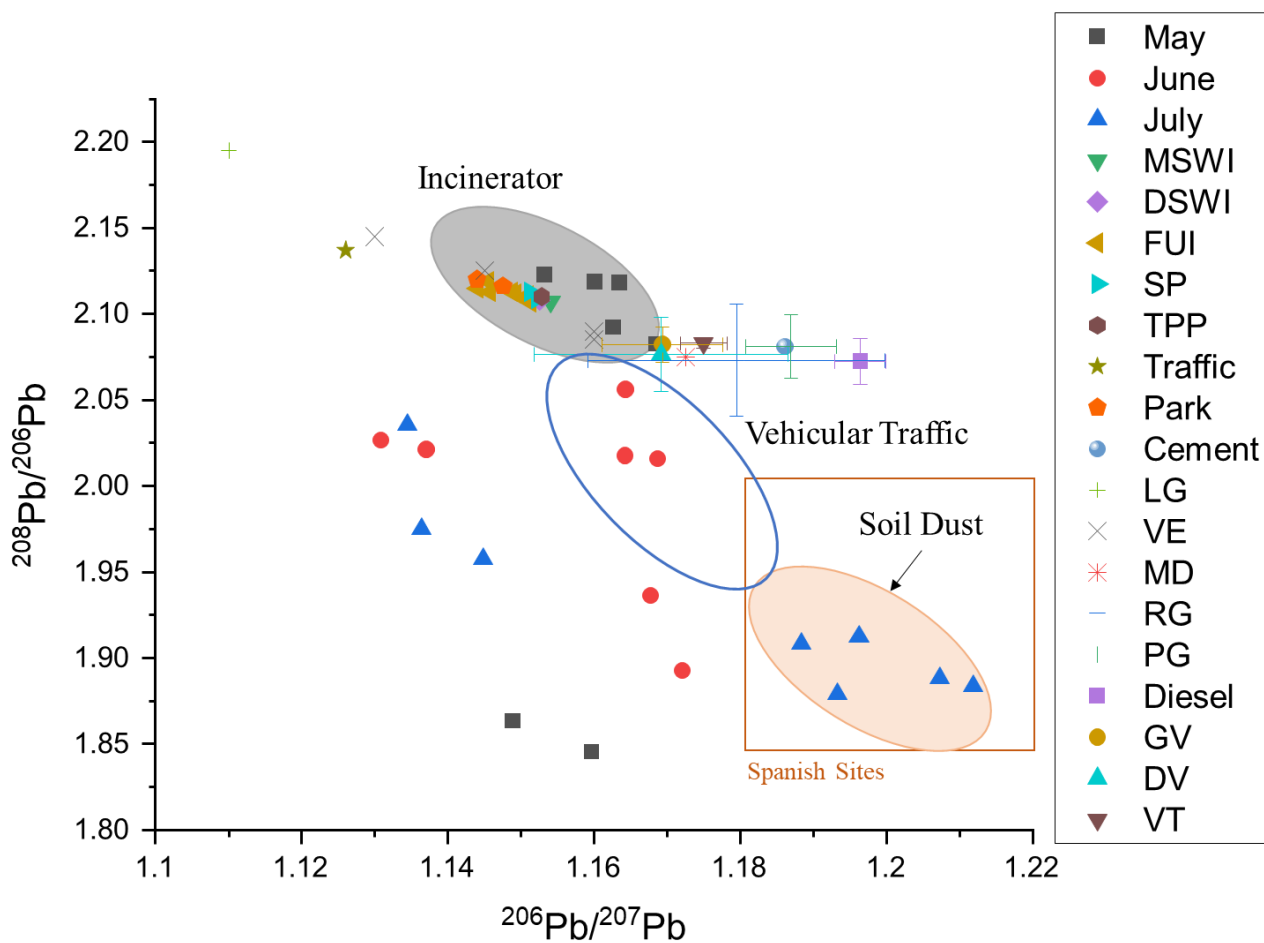
629 In addition, the isotopic composition of lead changes quickly depending on the different inputs for this
630 element, distance from industrial areas, traffic density, prevailing wind directions and rainfall intensity
631 (Simonetti et al., 2000).

632 In Europe, an important increase of the ²⁰⁶Pb/²⁰⁷Pb ratio (from 1.09 to 1.17) was observed from the end of
633 the 19th to the end of 20th century. This increase can be explained by several causes, such as a significant
634 import of ores with less radiogenic ratios, modifications in industrial practices, combustion process of coal
635 originating from different areas of the world (Bacon et al., 1996).

636 A further increase of the ²⁰⁶Pb/²⁰⁷Pb ratio was caused by the introduction of leaded gasoline throughout the
637 world. The subsequent decrease of the ²⁰⁶Pb/²⁰⁷Pb ratio (to 1.09) in the 1980s reflects the gradual
638 abandoning of leaded gasoline throughout Europe. These changes are associated with a decisive contraction
639 of atmospheric lead concentrations.

640 Values obtained in this work for the lead isotopes, in terms of ²⁰⁸Pb/²⁰⁶Pb and ²⁰⁶Pb/²⁰⁷Pb ratios, are
641 comparable to those found in the literature for countries from the Northern Hemisphere (De la Cruz et al.,

642 2009; Bollhöfer and Rosman, 2001) even if a higher radiogenic contribute was found respect to previous
 643 works performed in Venice between 1998 and 1999. Firstly, in that case the concentration of lead was
 644 higher (13-22 ng/m³) due to the presence of lead in gasoline in that period. Moreover, the values found for
 645 ²⁰⁸Pb/²⁰⁷Pb ratio (2.42-2.43) are comparable, denoting a variation only in the contribution of the radiogenic
 646 isotope (²⁰⁶Pb) (Bollhöfer and Rosman, 2001).
 647 Lead isotopic ratios determined in the PM₁₀ samples collected in TRM site are reported as ²⁰⁸Pb/²⁰⁶Pb vs
 648 ²⁰⁶Pb/²⁰⁷Pb ratios in figure 8.



649
 650 **Figure 8:** Plot of ²⁰⁸Pb/²⁰⁶Pb vs ²⁰⁶Pb/²⁰⁷Pb ratios for PM₁₀ samples collected in TRM site and in several
 651 source samples from literature data: MSWI (Carignan et al., 2005); DSWI – Domestic Solid Waste
 652 Incinerator, FUI – French Urban Incinerator, SP – Steel Plant, TPP – Thermal Power Plant, Traffic, Park,

653 *Cement (Lahd Geagea et al., 2008); LG – Loaded Gasoline, VE – Vehicle Exhaust, MD – Metallurgic Dust*
654 *(Xu et al., 2020); RG – Regular Gasoline, PG – Premium Gasoline, Diesel, GV – Gasoline Vehicular, DV*
655 *– Diesel Vehicular, VT – Vehicular Traffic (Gioia et al., 2017); Spanish Sites (Kylander et al., 2010).*

656
657 A partial separation of July samples from May and June samples can be observed; most of the July samples,
658 indeed, present low values for both $^{206}\text{Pb}/^{207}\text{Pb}$ and $^{208}\text{Pb}/^{206}\text{Pb}$ ratios. A distinction between May and June
659 samples is not evident, even if May samples show intermediate values for the $^{206}\text{Pb}/^{207}\text{Pb}$ ratios and a greater
660 variability in the values for $^{208}\text{Pb}/^{206}\text{Pb}$ ratios, whereas the June samples are characterized by higher values
661 for the $^{206}\text{Pb}/^{207}\text{Pb}$ ratios and intermediate values for $^{208}\text{Pb}/^{206}\text{Pb}$ ratios.

662 Thus, comparing these results with other studies (Widory et al., 2004; Komárek et al., 2006; Novák et al.,
663 2003; Teutsch et al., 2001; Carignan et al., 2005; Lahd Geagea et al., 2008; Guéguen et al., 2012; Gioia et
664 al., 2010, 2017; Zhao et al., 2019; Lee et al., 2019; Xu et al. 2020), it is possible to speculate a principally
665 geogenic contribution for lead in PM_{10} samples collected in July since the lead isotope ratios found in most
666 of these samples are more characteristic of European ores. Indeed, the $^{206}\text{Pb}/^{207}\text{Pb}$ ratios ranged from 1.8833
667 to 1.2119, with an average value of 1.1994, similar to the results reported by Kylander et al. (2010),
668 Kelepertzis et al. (2016) and Zhao et al. (2019), in which the natural end member of parent material showed
669 higher $^{206}\text{Pb}/^{207}\text{Pb}$ ratios compared with the anthropogenic-related sources. For example, the major soil dust
670 emitting areas on a global scale, including the Sahara–Sahel area (Abouchami and Zabel, 2003), Gobi desert
671 (Biscaye, et al., 1997) and European loess soils (Klaminder, et al., 2003; Sterckeman et al., 2006), have
672 $^{206}\text{Pb}/^{207}\text{Pb}$ ratios varying between 1.19 and 1.25. The PM_{10} samples collected in June, instead, seem be
673 more influenced by vehicular traffic ($^{206}\text{Pb}/^{207}\text{Pb}$ ratios ranged from 1.1308 to 1.1721, with the average
674 value of 1.1578). Indeed, these data fit well with $^{206}\text{Pb}/^{207}\text{Pb}$ ratios determined by Gioia et al. (2010 and
675 2017) for several traffic sources and suggest that the main source of lead in these samples is represented by
676 vehicular traffic. Finally, it is particularly noteworthy that most of the PM_{10} samples collected in May
677 display $^{208}\text{Pb}/^{206}\text{Pb}$ and $^{206}\text{Pb}/^{207}\text{Pb}$ ratios similar to values reported for several European MSWI plants

678 (Carignan et al, 2005; Geagea et al., 2008; Guéguen et al., 2012). The chemical and isotopic characterization
679 of Pb emitted by MSWI plants is not an easy task because of the extreme heterogeneity of waste materials
680 processed in these plants. Moreover, MSWI plants represent themselves a significant source of metals to
681 the atmosphere. Nevertheless, the Pb isotopic composition for this source, reported in the literature
682 (Carignan et al., 2005; Lahd Geagea et al., 2008 Guéguen et al., 2012), is fairly homogeneous and is defined
683 by a restricted range in $^{206}\text{Pb}/^{207}\text{Pb}$ and $^{208}\text{Pb}/^{206}\text{Pb}$ values, 1.148-1.158 and 2.101-2.114 respectively,
684 compared to other environmental samples. In conclusion, it is evident that the higher Pb content is not
685 indicative of a greater contribution of this element to PM_{10} due to the MSWI commissioning because, during
686 start-up phase, the lowest concentration for this element was observed in May (range: 0.54-2.27, mean:
687 1.17 ng/m^3) and it increased in June and July (range: 2.73-7.35, mean: 1.58 in June and range: 2.26-4.36,
688 mean: 3.16 in July). The commissioning of second line of combustion from 22 May to 5 June could be the
689 most likely explanation for the greater influence of incinerator emissions on PM_{10} , evidenced by the Pb
690 isotope ratios at the end of May. In July, when the MSWI plant has likely entered full capacity, it is possible
691 that the Pb isotope ratios represent the typical sources influencing the PM_{10} in the investigated area, i.e.
692 vehicular traffic and soil dust.

693

694 **Conclusions**

695

696 In conclusion, vehicular traffic was identified as the main atmospheric pollution source for PM_{10} samples
697 collected near Turin MSWI plant. EFs and element concentrations are comparable with those reported for
698 other sites located in the city of Turin confirming that the installation of MSWI plant did not lead to an
699 overall increase in polluting emissions into the atmosphere. The elements moderately or highly enriched
700 (Cr, Ni, Cu, Zn, As, Mo, Cd and Pb) seem to arise mainly from vehicle emissions which likely increased
701 in this area after the opening of the MSWI plant due to heavier traffic of trucks carrying the wastes. This
702 source of tropospheric pollution affects also lead concentration, as confirmed by lead isotope ratios

703 determined by a method that was developed and optimized using an experimental design approach..
704 However, a possible crustal contribution in July and a possible influence of the incinerator in May have
705 been highlighted taking into account the lead isotope ratios determined in PM₁₀ samples collected in these
706 two months.
707 Further studies about lead isotope ratios and PM₁₀ elemental composition should be done in the same area
708 of sampling during incinerator activity for defining a possible long-term impact of the plant in the Turin
709 suburban area.

710

711 **References**

712

713 Abouchami W., Zabel M., 2003. Climate forcing of the Pb isotope record of terrigenous input into the
714 Equatorial Atlantic. *Earth Planet. Sci. Lett.* 213, 221–234. DOI: 10.1016/S0012-821X(03)00304-2.

715 Amato, F. *Non-exhaust emissions*; Elsevier: 2018.

716 Arpa Piemonte, *Rapporto di sintesi sui dati prodotti dalla stazione di monitoraggio della qualità dell'aria*
717 *ubicata nel Comune di Beinasco – Giardino Pubblico Aldo Mei, di proprietà di TRM S.p.A. Anno 2013.*

718 Arpa Piemonte, 2013. *Uno sguardo all'aria.*

719 Arpa Piemonte, 2014. *Uno sguardo all'aria.*

720 Arpa Piemonte, 2015. *Uno sguardo all'aria.*

721 Arpa Piemonte, 2016. *Uno sguardo all'aria.*

722 Arpa Piemonte, 2017. *Uno sguardo all'aria.*

723 Arpa Piemonte, 2018. *Uno sguardo all'aria.*

724 Bacon J.R., Jones K.C., McGrath S.P., Johnston A.E., 1996. Isotopic character of lead deposited from the
725 atmosphere at a grassland site in the United Kingdom since 1860. *Environ. Sci. Technol.* 30, 2511–2518.
726 DOI: 10.1021/es950839s.

727 Biasioli M., Barberis R., Ajmone-Marsan F., 2006. The influence of a large city on some soil properties
728 and metals content. *Sci. Total Environ.* 356, 154-164. DOI: 10.1016/j.scitotenv.2005.04.033.

729 Birmili W., Allen A.G., Bary F., Harrison R.M., 2006. Trace metal concentrations and water solubility in
730 size-fractionated atmospheric particles and influence of road traffic. *Environ.Sci.Technol.* 40, 1144-1153.
731 DOI: 10.1021/es0486925.

732 Biscaye P.E., Grousset F.E., Revel M., Gaast V.S., Zielinski G.A., Vaars A., Kukla G., 1997. Asian
733 provenance of glacial dust (stage 2) in the Greenland Ice Sheet Project 2 ice core Summit Greenland. *J.*
734 *Geophys. Res.* 102, 26765–26781. DOI: 10.1029/97JC01249.

735 Bollhöfer A., Rosman K.J.R., 2000. Isotopic source signatures for atmospheric lead: The Southern
736 Hemisphere. *Geochim. Cosmochim. Acta* 64, 3251–3262. DOI: 10.1016/S0016-7037(00)00436-1.

737 Bollhöfer A., Rosman K.J.R., 2001. Isotopic source signatures for atmospheric lead: The Northern
738 Hemisphere. *Geochim. Cosmochim. Acta.* 65, 1727-1740. DOI: 10.1016/S0016-7037(00)00630-X.

739 Bonifacio E., Falsone G., Piazza S., 2010. Linking Ni and Cr concentrations to soil mineralogy: does it help
740 to assess metal contamination when the natural background is high? *J. Soils Sediments* 10, 1475-1486.
741 DOI: 10.1007/s11368-010-0244-0.

742 Carignan J., Libourel G., Cloquet C., Le Forestier L., 2005. Lead isotopic composition of fly ash and flue
743 gas residues from municipal solid waste combustors in France: implications for atmospheric lead source
744 tracing. *Environ. Sci. Technol.* 39, 2018-2024. DOI: 10.1021/es048693x.

745 Cohen J., Cohen P., West S.G., Aiken L.S., 2003. *Applied multiple regression/correlation analysis for the*
746 *behavioral sciences.* 3rd ed. Lawrence Erlbaum Associates, Inc., Mahwah, New Jersey.

747 Conca E., Malandrino M., Giacomino A., Inaudi P., Buoso S., Bande S., Sacco M., Abollino O., 2020.
748 Contribution of the incinerator to the inorganic composition of the PM₁₀ collected in Turin, Atmosphere-
749 Basel, 11, 400. DOI: 10.3390/atmos11040400.

750 Councill T.B., Duckenfield K.U., Landa E.R., Callender E., 2004. Tire-wear particles as a source of zinc
751 to the environment. Environ. Sci. Technol., 38, 4206-4214. DOI: 10.1021/es034631f.

752 Decreto Ministeriale n 60 02/04/2002 from Council Directive 1999/30/EC of 22 April 1999.

753 De la Cruz M.T., Laborda F., Callén M.S., López J.M., Mastral A.M., 2009. Study of Pb sources by Pb
754 isotope ratios in the airborne PM₁₀ of Zaragoza, Spain. J. Environ. Monit. 11, 2052-2057. DOI:
755 10.1039/b912274e.

756 Directive 2000/76/EC of the European Parliament and of the Council of 28 December 2010 on the
757 incineration of waste (the WI Directive).

758 Directive 2008/50/EC of the European Parliament and of the Council of 21 May 2008 on ambient air quality
759 and cleaner air for Europe.

760 D.Lgs. 155, 2010. Official Gazette of the Italian Republic, 216.

761 European Environment Agency (EEA), 2013. Air quality in Europe – 2013 report 9/2013.

762 European Environment Agency (EEA), 2015. Air quality in Europe – 2015 report 5/2015.

763 Fan J., Yue X.Y., Jing Y., Chen Q., Wang S.G., 2014. Online monitoring of water-soluble ionic composition
764 of PM₁₀ during early summer over Lanzhou City. J. Environ. Sci. 26, 353–361. DOI: 10.1016/S1001-
765 0742(13)60431-3.

766 Flament P., Bertho M.L., Deboudt K., Veron A., Puskaric E., 2002. European isotopic signatures for lead
767 in atmospheric aerosols: a source apportionment based upon Pb-206/Pb-207 ratios. Sci. Total. Environ.
768 296, 35–57. DOI: 10.1016/S0048-9697(02)00021-9.

769 Font A., de Hoogh K., Leal-Sanchez M., Ashworth D.C., Brown R.J.C., Hansell A.L., Fuller G.W., 2015.
770 Using metal ratios to detect emissions from municipal waste incinerators in ambient air pollution data.
771 Atmos. Environ. 113, 177-186. DOI: 10.1016/j.atmosenv.2015.05.002.

772 Gao J.J., Tian H.Z., Cheng K., Lu L., Zheng M., Wang S.X., Hao J.M., Wang K., Hua S.B., Zhu C.Y.,
773 Wang Y., 2015. The variation of chemical characteristics of PM_{2.5} and PM₁₀ and formation causes during
774 two haze pollution events in urban Beijing, China. Atmos. Environ. 107, 1-8. DOI:
775 10.1016/j.atmosenv.2015.02.022.

776 Gerhardsson L., 2004. Lead In: Merian E., Anke M., Ihnat M., Stoepler M. (Eds.), Elements and their
777 compounds in the environment, WILEY-VCH Verlag GmbH&Co. KGaA, Weinheim, 879-900.

778 Gholampour A., Nabizadeh R., Hassanvand M.S., Taghipour H., Rafee M., Alizadeh Z., Faridi S., Mahvi
779 A.H., 2016. Characterization and source identification of trace elements in airborne particulates at urban
780 and suburban atmospheres of Tabriz, Iran. Environ. Sci. Pollut. Res. Int. 23, 1703-1713. DOI:
781 10.1007/s11356-015-5413-7.

782 Gioia, S.M.C.L., Babinski, M., Weiss, D.J., Kerr, A.A.F.S., 2010. Insights into the dynamics and sources
783 of atmospheric lead and particulate matter in São Paulo, Brazil, from high temporal resolution sampling.
784 Atmos. Res. 98, 478-485. DOI: 10.1016/j.atmosres.2010.08.016.

785 Gioia S.M.C.L., Babinski M., Weiss D.J., Spiro B., Kerr A.A.F.S., Veríssimo T.G., Ruiz I., Prates J.C.M.,
786 2017. An isotopic study of atmospheric lead in a megacity after phasing out of leaded gasoline Atmos.
787 Environ. 149, 70-83. DOI: 10.1016/j.atmosenv.2016.10.049.

788 Guéguen F., Stille P., Lahd Geagea M., Perrone T., Chabaux F., 2012. Atmospheric pollution in an urban
789 environment by tree bark biomonitoring – Part II: Sr, Nd and Pb isotopic tracing, Chemosphere 86, 641–
790 647. DOI: 10.1016/j.chemosphere.2011.11.008.

791 Harrison R.M., Jones A.M., Gietl J., Yin J., Green D.C., 2012. Estimation of the contributions of brake
792 dust, tire wear, and resuspension to non-exhaust traffic particles derived from atmospheric measurements.
793 Environ. Sci. Technol. 46, 6523-6529. DOI: 10.1021/es300894r.
794 <http://trm.to.it/> (Date of access: 12 November 2020).
795 <https://umetrics.com/product/modde> (Date of access: 20 October 2014).
796 International Agency for Research on Cancer (IARC), 2012. IARC monographs on evaluation of
797 carcinogenic risk of chemicals to humans. A review of human carcinogens: arsenic, metals, fibres, and
798 dusts, Vol. 100 C. Lyon, France: World Health Organization.
799 Kelepertzis E., Komárek M., Argyrakia A., Šillerová H., 2016. Metal(loid) distribution and Pb isotopic
800 signatures in the urban environment of Athens, Greece. Environ. Pollut. 213, 420-431. DOI:
801 10.1016/j.envpol.2016.02.049.
802 Klaminder J., Renberg I., Bindler R., Emteryd O., 2003. Isotopic trends and background fluxes of
803 atmospheric lead in northern Europe: analyses of three ombrotrophic bogs from south Sweden. Global
804 Biogeochem. Cy. 17, 1019. DOI: 10.1029/2002GB001921.
805 Komárek M., Chrastný V., Ettler V., Tlustoš P., 2006. Evaluation of extraction/digestion techniques used
806 to determine lead isotopic composition in forest soils. Anal. Bioanal. Chem. 385, 1109–1115. DOI:
807 10.1007/s00216-006-0543-x.
808 Komarek M., Ettler V., Chrastný V., Mihaljevic M., 2008. Lead isotopes in environmental sciences: a
809 review. Environ. Int. 34, 562-577. DOI: 10.1016/j.envint.2007.10.005
810 Kylander M.E., Klaminder J., Bindler R., Weiss D.J., 2010. Natural lead isotope variations in the
811 atmosphere. Earth Planet. Sc. Lett. 290, 44–53. DOI: 10.1016/j.epsl.2009.11.055.

812 Lahd Geagea M., Stille P., Gauthier - Lafaye F., Millet M., 2008. Tracing of industrial aerosol sources in
813 an urban environment using Pb, Sr, and Nd isotopes. *Environ. Sci. Technol.* 42, 692–698. DOI:
814 10.1021/es071704c.

815 Lai A.M., Shafer M.M., Dibb J.E., Polashenski C.M., Schauer J.J., 2017. Elements and inorganic ions as
816 source tracers in recent Greenland snow. *Atmos. Environ.* 164: 205-215. DOI:
817 10.1016/j.atmosenv.2017.05.048.

818 Lee S., Shin D., Han C., Choi K.S., Hur S.D., Lee J., Byun D.S., Kim Y.T., Hong S., 2019. Characteristic
819 concentrations and isotopic composition of airborne lead at urban, rural and remote sites in western Korea.
820 *Environ. Pollut.* 254, 113050. DOI: 10.1016/j.envpol.2019.113050.

821 Li T.C., Yuan C.S., Lo K.C., Hung C.H., Wu S.P, Tong C., 2015. Seasonal variation and chemical
822 characteristics of atmospheric particles at three islands in the Taiwan strait. *Aerosol Air Qual. Res.* 15,
823 2277–2290. DOI: 10.4209/aaqr.2015.03.0153.

824 Lucarelli F., Barrera V., Becagli S., Chiari M., Giannoni M., Nava S., Traversi R., Calzolari G., 2019.
825 Combined use of daily and hourly data sets for the source apportionment of particulate matter near a waste
826 incinerator plant. *Environ. Pollut.* 247, 802-811. DOI: 10.1016/j.envpol.2018.11.107.

827 Lundstedt T., Seifert E., Abramo L., Thelin B., Nystrom A., Pettersen J., Bergman R., 1998. Experimental
828 design and optimization. *Chemom. Intell. Lab. Syst.* 42, 3-40.

829 Malandrino M., Di Martino M., Ghiotti G., Geobaldo F., Grosa M.M., Giacomino A., Abollino O., 2013.
830 Inter-annual and seasonal variability in PM10 samples monitored in the city of Turin (Italy) from 2002 to
831 2005. *Microchem. J.* 107, 76-85. DOI: 10.1016/j.microc.2012.05.026.

832 Meyer P.A., Brown M.J., Falk H. 2008. Global approach to reducing lead exposure and poisoning. *Mutat.*
833 *Res. Rev. Mutat. Res.* 659, 166-175. DOI: 10.1016/j.mrrev.2008.03.003. Novák M., Emmanuel S., Vile
834 M.A., Erel Y., Véron A., Pačes T., Wieder R.K., Vaněček M, Štěpánová M, Břízová E., Hovorka J., 2003.

835 Origin of lead in eight European peat bogs determined from isotope ratios, strengths, and operation times
836 of regional pollution sources. *Environ. Sci. Technol.* 37, 437–445. DOI: 10.1021/es0200387.

837 Ochsenkühn K.M., Lyberopoulou T., Koumarianou G., Ochsenkühn-Petropoulou M., 2008. Ion
838 chromatographic and spectrometric determination of water-soluble compounds in airborne particulates, and
839 their correlations in an industrial area in Attica, Greece. *Microchim. Acta.* 160, 485–492. DOI:
840 10.1007/s00604-007-0830-z.

841 Pacyna E.G., Pacyna J.M., Fudala J., Strzelecka-Jastrzab E., Hlawiczka S., Panasiuk D., Nitter S., Pregger
842 T., Pfeiffer H., Friedrich R., 2007. Current and future emissions of selected heavy metals to the atmosphere
843 from anthropogenic sources in Europe. *Atmos. Environ.* 41, 8557e8566. DOI:
844 10.1016/j.atmosenv.2007.07.040.

845 Padoan E., Malandrino M., Giacomino A., Grosa M., Lollobrigida F., Martini S., Abollino O., 2016. Spatial
846 distribution and potential sources of trace elements in PM10 monitored in urban and rural sites of Piedmont
847 Region. *Chemosphere* 145, 495–507. DOI: 10.1016/j.chemosphere.2015.11.094.

848 Pakkanen T., Loukkola K., Kohonen C., Aurela M., Mäkelä T., Hillamo, R., Aarnio P., Koskentalo T.,
849 Kousa A., Maenhaut W., 2001. Sources and chemical composition of atmospheric fine and coarse particles
850 in the Helsinki area. *Atmos. Environ.* 35, 5381-5391. DOI: 10.1016/S1352-2310(01)00307-7.

851 Panepinto D., Zanetti M.C., 2018. Municipal solid waste incineration plant: A multi-step approach to the
852 evaluation of an energy-recovery configuration. *Waste Manage. (Oxford)* 73, 332-341, DOI:
853 10.1016/j.wasman.2017.07.036.

854 Poschl U., 2005. Atmospheric aerosols. Composition, transformation, climate and health effects. *Angew.*
855 *Chem. Int. Edit.* 44, 7520-7540. DOI: 10.1002/anie.200501122.

856 Raffaelli K., Deserti M., Stortini M., Amorati R., Vasconi M., Giovannini G., 2020. Improving air quality
857 in the Po Valley, Italy: some results by the LIFE-IP-PREPAIR Project. *Atmosphere* 11, 429.
858 DOI:10.3390/atmos11040429.

859 Rokach L., Maimon O., 2005. Clustering methods. Data mining and knowledge discovery handbook.
860 Springer, Boston, US.

861 Sakata M., Kurata M., Tanaka, N., 2000. Estimating contribution from municipal solid waste incineration
862 to trace metal concentrations in Japanese urban atmosphere using lead as a marker element. *Geochem. J.*
863 34, 23-32. DOI: 10.2343/geochemj.34.23.

864 Simonetti A., Gariépy C., Carignan J., 2000. Pb and Sr isotopic compositions of snowpack from Québec,
865 Canada: inferences on the sources and deposition budgets of atmospheric heavy metals. *Geochim*
866 *Cosmochim. Acta* 64, 5–20. DOI: 10.1016/S0016-7037(99)00207-0.

867 Sterckeman T., Douay F., Baize D., Fourrier H., Proix N., Schvartz C., Carignan J., 2006. Trace element
868 distributions in soils developed in loess deposits from northern France. *Eur. J. Soil Sci.* 57, 392–410. DOI:
869 10.1111/j.1365-2389.2005.00750.x.

870 Tahri M., Benchrif A., Bounakhla M., Benyaich F., Noack Y., 2017. Seasonal variation and risk assessment
871 of PM_{2.5} and PM_{2.5-10} in the ambient air of Kenitra, Morocco. *Environ. Sci.-Proc. Imp.* 19: 1427-1436.
872 DOI: 10.1039/c7em00286f.

873 Teutsch N., Erel Y., Halicz L., Banin A., 2001. Distribution of natural and anthropogenic lead in
874 Mediterranean soils. *Geochim. Cosmochim. Acta* 65, 2853–2864. DOI: 10.1016/S0016-7037(01)00607-X.

875 Tong S., von Schirnding Y.E.; Prapamontol T., 2000. Environmental lead exposure: a public health problem
876 of global dimensions. *Bull. World Health Organ.* 78, 1068-1077.

877 Vinceti M., Malagoli C., Teggi S., Fabbi S., Goldoni C., De Girolamo G., Ferrari P., Astolfi G., Rivieri F.,
878 Bergomi M., 2008. Adverse pregnancy outcomes in a population exposed to the emissions of a municipal
879 waste incinerator. *Sci. Total Environ.* 407, 116–121. DOI: 10.1016/j.scitotenv.2008.08.027.

880 Wedepohl H., 1995. The composition of the continental crust. *Geochim. Cosmochim. Acta* 59, 1217-1232.

881 Widory D., Roy S., Le Moullec Y., Goupil G., Cocherie A., Guerrot C., 2004. The origin of atmospheric
882 particles in Paris: a view through carbon and lead isotopes. *Atmos. Environ.* 38, 953–961. DOI:
883 10.1016/j.atmosenv.2003.11.001.

884 Widory D., Liu X.D., Dong S.P., 2010. Isotopes as tracers of sources of lead and strontium in aerosols (TSP
885 & PM_{2.5}) in Beijing. *Atmos. Environ.* 44, 3679-3687. DOI: 10.1016/j.atmosenv.2010.06.036.

886 World Health Organization (WHO), 2007. Population health and waste management: scientific data and
887 policy options. Report of a WHO workshop, Rome, Italy. Copenhagen, Denmark: Regional Office for
888 Europe.

889 Xu L.L., Chen X.Q., Chen J.S., Zhang F.W., He C., Zhao J.P., Yin L.Q., 2012. Seasonal variations and
890 chemical compositions of PM_{2.5} aerosol in the urban area of Fuzhou, China. *Atmos. Res.* 104-105, 264-
891 272. DOI: 10.1016/j.atmosres.2011.10.017.

892 Xu H.M., He K.L., Feng R., Shen Z.X., Cao J.J., Liu S.X., Ho K.F., Huang R.-J., Guinot B., Wang Q.Y.,
893 Zhou J.M., Shen M. X., Xiao S., Zhouf B.H., Sonke J.E., 2020. Metallic elements and Pb isotopes in PM_{2.5}
894 in three Chinese typical megacities: spatial distribution and source apportionment. *Environ. Sci.: Processes*
895 *Impacts* 22, 1718-1730. DOI: 10.1039/d0em00174k.

896 Yadav R., Sahu L.K., Jaaffrey S.N.A., Beig G., 2014. Distributions of ozone and related trace gases at an
897 urban site in western India. *J. Atmos. Chem.* 71, 125–144. DOI: 10.1007/s10874-014-9286-9.

898 Zhang J., Peng J., Song C., Ma C., Men Z., Wu J., Wu L., Wang T., Zhang X., Tao S., Gao S., Hopke P.K.,
899 Mao H., 2020. Vehicular non-exhaust particulate emissions in Chinese megacities: Source profiles, real-
900 world emission factors, and inventories. *Environ. Pollut.* 266, 115268 DOI: 10.1016/j.envpol.2020.115268.

901 Zhao Y., Yu R.L., Hu G.R., Lin X.H., Liu X.R., 2017. Chemical characteristics and Pb isotopic
902 compositions of PM_{2.5} in Nanchang, China. *Particuology* 32, 95–102. DOI: 10.1016/j.partic.2016.07.009.

903 Zhao L., Hu G., Yan Y., Yu R., Cui J., Wang X., Yan Y., 2019. Source apportionment of heavy metals in
904 urban road dust in a continental city of eastern China: Using Pb and Sr isotopes combined with multivariate
905 statistical analysis. *Atmos. Environ.* 201, 201–211. DOI: 10.1016/j.atmosenv.2018.12.050.

906 Zhou J.B., Xing Z.Y., Deng J.J., Du K., 2016. Characterizing and sourcing ambient PM_{2.5} over key
907 emission regions in China I: water-soluble ions and carbonaceous fractions. *Atmos. Environ.* 135, 20-30.
908 DOI: 10.1016/j.atmosenv.2016.03.054.

909 Zhou J.M., Shen M.X., Xiao S., Zhou B.H., Sonke J.E., 2020. Metallic elements and Pb isotopes in PM_{2.5}
910 in three Chinese typical megacities: spatial distribution and source apportionment. *Environ. Sci.-Proc. Imp.*
911 22, 1718-1730. DOI: 10.1039/d0em00174k.

912 Zhu Y., Kashiwagi K., Sakaguchi M., Aoki M., Fujimori E., Haraguchi H., 2006. Lead isotopic
913 compositions of atmospheric suspended particulate matter in Nagoya City as measured by HR-ICP-MS. *J.*
914 *Nucl. Sci. Technol.* 43, 474-478. DOI: 10.3327/jnst.43.474.

SUPPLEMENTARY MATERIAL

Table 1S. Meteorological data, PM₁₀ and PM_{2.5} mass concentrations ($\mu\text{g}/\text{m}^3$), and NO and NO₂ atmospheric concentrations ($\mu\text{g}/\text{m}^3$) of the samples collected during start-up phase: a) from 09 May 2013 to 17 June 2013 and b) from 18 June 2013 to 16 July 2013.

a)	PM _{2.5}	PM ₁₀	NO	NO ₂	WS avg (m/s)	WS max (m/s)	h avg (m)	h max (m)	T avg (°C)	b)	PM _{2.5}	PM ₁₀	NO	NO ₂	WS avg (m/s)	WS max (m/s)	h avg (m)	h max (m)	T avg (°C)
09/05	n.a.	21	129	603	1.03	2.15	688	1419	19.08	18/06	22	36	74	677	0.68	1.07	618	1276	27.13
10/05	10	14	47	459	1.06	1.85	611	1305	16.31	19/06	21	33	64	618	0.73	1.23	547	1210	26.1
11/05	8	9	110	327	0.82	1.54	625	1370	17.27	20/06	17	27	131	784	0.92	1.77	559	1203	21.47
12/05	5	8	37	126	1.00	2.24	737	1465	17.79	21/06	15	21	104	485	0.86	1.42	700	1386	21.40
13/05	8	13	268	782	0.86	1.76	647	1316	16.56	22/06	12	18	65	411	1.07	1.58	732	1457	22.43
14/05	12	16	72	597	1.04	2.15	686	1380	16.17	24/06	4	10	62	503	1.15	2.82	837	1562	21.45
15/05	7	11	39	501	1.66	2.60	642	1281	12.08	25/06	5	8	152	1072	0.79	1.25	783	1567	20.58
16/05	3	6	99	620	1.83	2.73	562	1186	11.41	26/06	6	12	138	838	0.87	1.57	786	1555	20.55
25/05	5	5	46	336	1.34	2.47	567	1230	10.58	27/06	11	17	56	656	1.22	2.03	730	1462	17.44
26/05	6	5	71	438	1.19	1.74	631	1262	14.24	28/06	11	15	68	530	0.88	1.47	678	1401	16.46
27/05	9	11	99	509	1.16	2.54	607	1313	15.41	29/06	13	21	166	777	0.84	1.60	696	1433	18.22
28/05	11	20	77	396	0.88	1.79	561	1246	14.28	30/06	11	18	n.a.	593	0.85	1.65	705	1452	21.61
29/05	5	6	88	498	1.28	1.94	685	1360	12.37	02/07	12	23	101	476	0.76	1.66	790	1949	22.67
30/05	5	9	255	670	1.16	1.83	585	1279	14.32	03/07	14	21	n.a.	595	0.88	1.71	708	1444	21.00
31/05	6	6	235	598	1.28	1.86	602	1278	16.62	04/07	15	23	241	761	0.78	1.37	717	1422	23.40
01/06	9	14	102	433	0.87	1.42	594	1269	19.34	05/07	16	26	117	914	0.62	1.21	757	1507	25.30
02/06	7	49	58	422	0.88	1.43	726	1438	21.14	06/07	18	27	42	490	0.87	1.92	725	1492	25.36
03/06	16	19	n.a.	849	0.79	1.50	670	1320	18.27	07/07	15	21	11	326	1.08	1.63	658	1405	25.31
04/06	15	21	132	942	0.69	1.05	630	1236	19.17	08/07	15	22	93	490	0.76	1.36	662	1376	24.65
05/06	18	26	102	923	0.64	1.44	601	1326	19.14	09/07	11	16	117	542	0.81	1.27	592	1301	23.86
08/06	14	21	76	652	0.81	1.93	579	1297	20.22	10/07	13	21	123	815	0.62	1.10	666	1383	24.39
09/06	8	13	42	303	1.16	2.50	607	1209	15.33	11/07	14	23	56	553	0.74	1.79	711	1388	25.23
10/06	8	11	119	522	0.83	1.31	587	1220	17.59	12/07	18	29	48	529	0.75	1.95	682	1326	23.71
11/06	9	15	181	909	0.67	1.21	678	1400	21.14	13/07	21	31	n.a.	466	0.85	1.66	671	1293	24.22
14/06	20	33	68	735	0.83	1.75	730	1380	23.73	14/07	16	19	32	316	0.70	1.23	639	1370	23.95
15/06	21	32	51	548	1.02	2.05	739	1459	23.50	15/07	17	22	187	708	0.51	0.91	663	1428	25.24
16/06	16	23	45	331	1.03	1.50	719	1417	24.38	16/07	20	27	43	470	0.94	1.69	649	1375	24.95
17/06	19	31	107	729	0.67	1.14	615	1255	26.18										

WS avg = average wind speed; WS max = maximum wind speed; WD = wind direction; h avg = average mixing height; h max = maximum mixing height; T avg = average temperature.

Table 2S. Experimental conditions, limits of detection (LOD) and sample blank concentrations of the analytes determined by ICP-AES.

Analyte	LOD ($\mu\text{g/L}$)	Sample Blank A ($\mu\text{g/L}$)	Sample Blank B ($\mu\text{g/L}$)
Al 396.153	8.1	45	46
Ca 317.933	40.8	100	90
Fe 238.204	39.8	< LOD	< LOD
K 769.896	5.2	30	20
Mg 285.213	8.6	32	31
Mn 257.610	0.22	2.1	1.0
K 769.896	5.2	30	20

A: Millipore© filters; B: Munktell filters

Table 3S. Experimental conditions, limits of detection (LOD) and sample blank concentrations of the analytes determined by SF-ICP-MS

Analyte	LOD (ng/L)	Sample Blank A (ng/L)	Sample Blank B (ng/L)
Ti47(LR)	754	3,860	1,030
V51(LR)	12	58	90
Cr53(LR)	48	834	760
Co59(MR)	7.0	8.7	< LOD
Ni60(MR)	41	240	350
Cu63(LR)	583	< LOD	< LOD
Zn66(MR)	1,450	3,860	3,220
As75(LR)	13	< LOD	< LOD
Sn118(LR)	3.0	< LOD	< LOD
Zr90(LR)	12	660	620
Mo96(MR)	21	390	340
Cd111(LR)	6.0	9.6	< LOD

Ba138(LR)	253	910	1,360
La139(MR)	5.7	62	60
Ce140(MR)	2.0	260	300
Tl203(MR)	14	< LOD	< LOD
Pb208(LR)	13	68	53

LR = Low Resolution; MR = Medium Resolution; A: Millipore© filters; B: Munktell filters

Table 4S. Limits of detection (LOD) and sample blank concentrations of water-soluble ions determined by IC.

Analyte	LOD (µg/L)	Sample Blank A (µg/L)	Sample Blank B (µg/L)
Cl ⁻	50	< LOD	< LOD
NO ₃ ⁻	500	< LOD	< LOD
SO ₄ ²⁻	800	< LOD	< LOD
Na ⁺	250	< LOD	< LOD
K ⁺	200	< LOD	< LOD
Mg ²⁺	150	< LOD	< LOD
Ca ²⁺	900	< LOD	< LOD
NH ₄ ⁺	100	< LOD	< LOD

A: Millipore© filters; B: Munktell filters

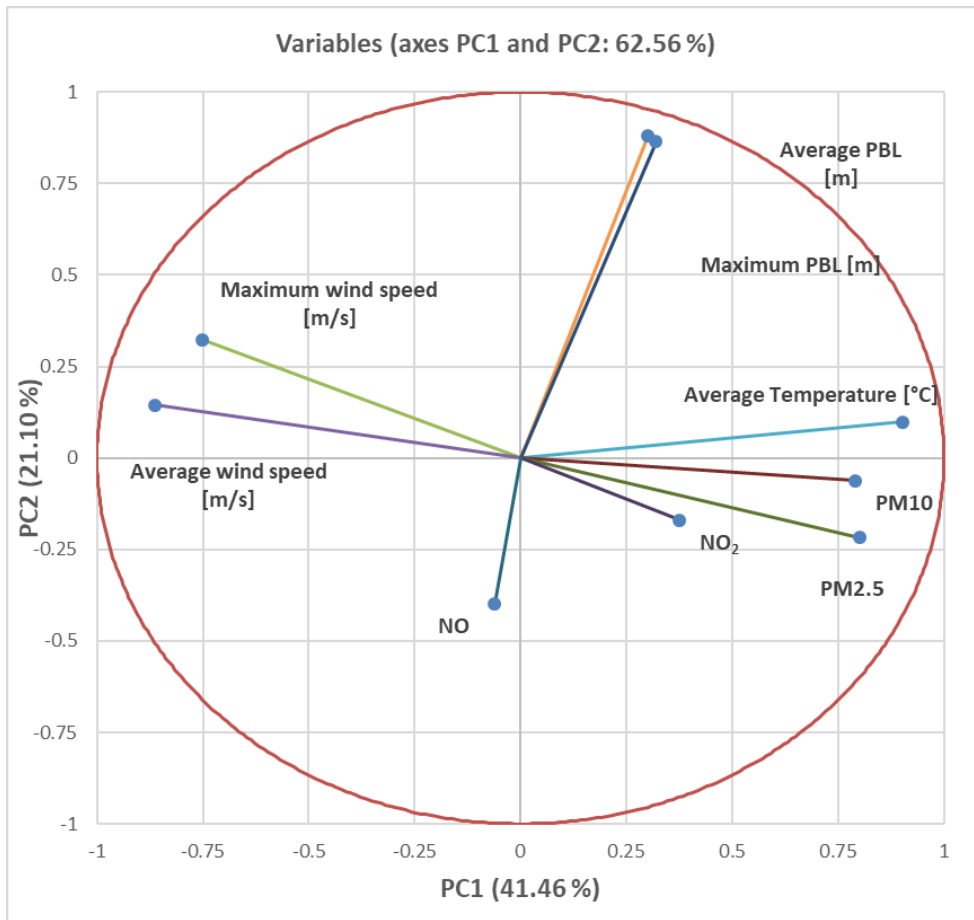


Figure 1S. Loadings from PCA (Principal Components Analysis).

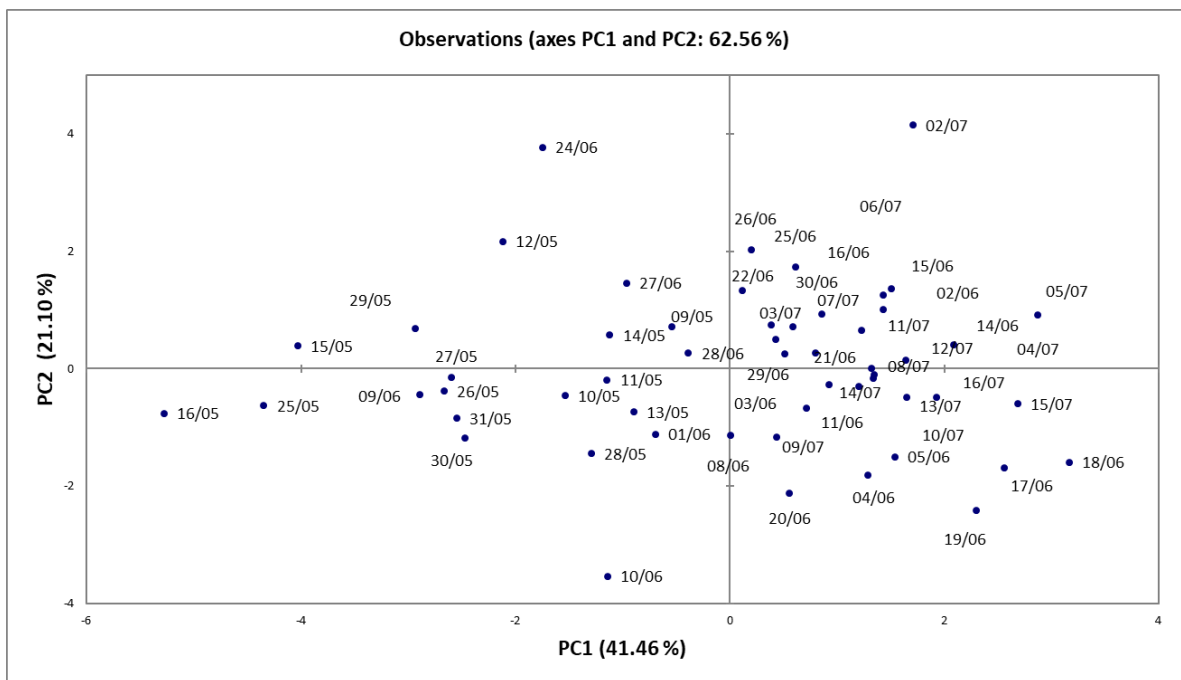


Figure 2S. Scores from PCA (Principal Components Analysis).

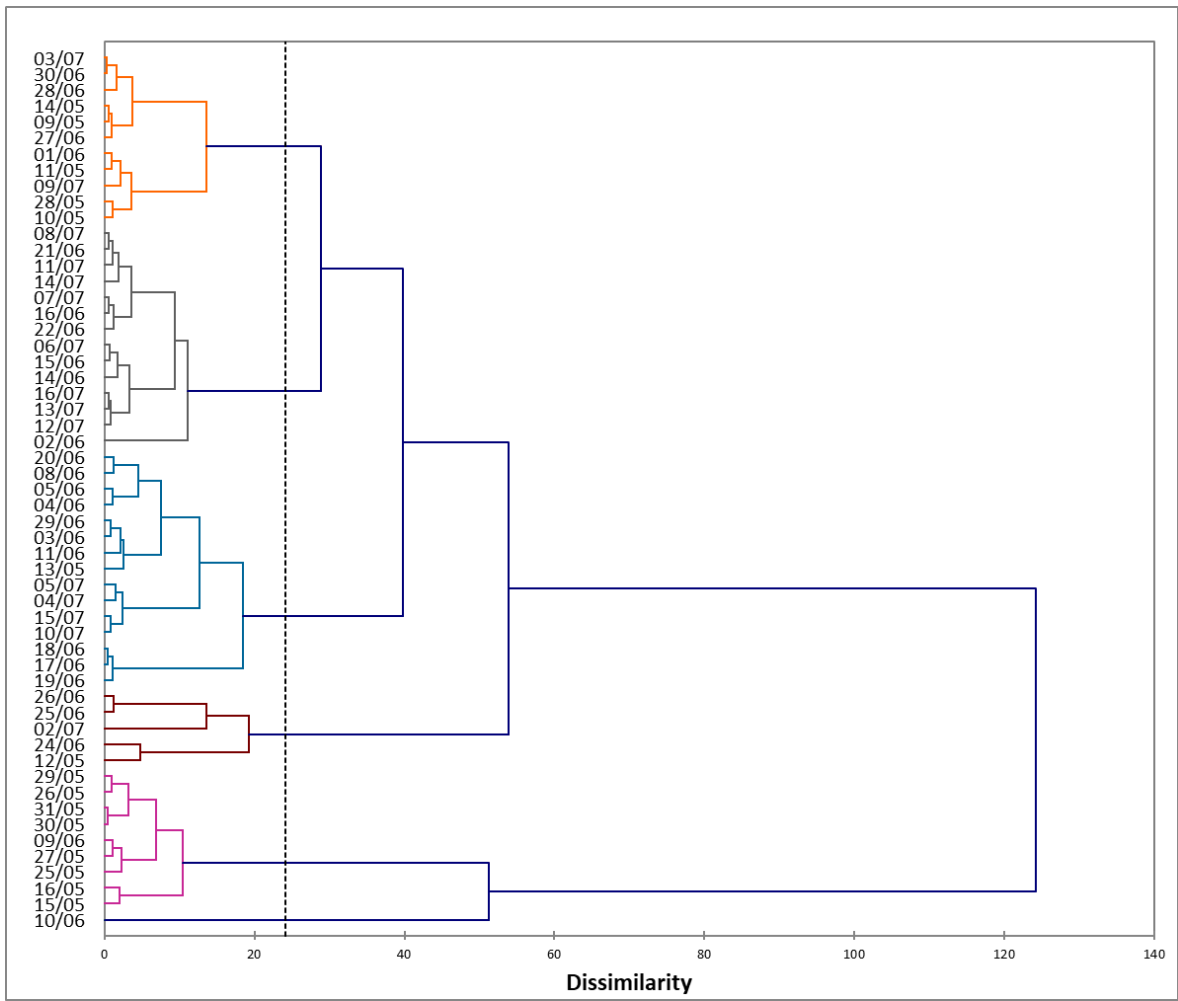


Figure 3S. Dendrogram of the samples from HCA (Hierarchical Cluster Analysis).

Table 5S. Water-soluble ionic components and major element concentrations in PM₁₀ samples. All the results are expressed in ng/m³, except NH₄⁺, NO₃⁻ and SO₄²⁻ which are expressed in µg/m³.

	Al	Ca	Ca ²⁺	Cl ⁻	Fe	K	K ⁺	Mg	Mg ²⁺	Na	Na ⁺	NH ₄ ⁺	NO ₃ ⁻	SO ₄ ²⁻
25 May	108 ± 1	178 ± 7	191 ± 8	< 19	200 ± 3	36 ± 2	40 ± 2	88 ± 2	12.7 ± 0.4	< SB	31 ± 1	0.26 ± 0.01	5.1 ± 0.2	0.64 ± 0.02
26 May	127 ± 4	147 ± 5	103 ± 3	< 19	233 ± 1	76.5 ± 0.2	84 ± 3	85.8 ± 0.2	10.6 ± 0.5	15 ± 5	29 ± 1	0.17 ± 0.01	4.9 ± 0.2	0.253 ± 0.007
27 May	230 ± 30	350 ± 40	280 ± 10	320 ± 10	340 ± 30	140 ± 20	100 ± 4	260 ± 30	116 ± 4	840 ± 30	950 ± 40	0.39 ± 0.01	19.6 ± 0.9	2.1 ± 0.1
28 May	217 ± 4	340 ± 20	330 ± 20	42 ± 1	332 ± 5	117 ± 3	105 ± 4	230 ± 4	86 ± 4	520 ± 20	680 ± 20	0.78 ± 0.02	27 ± 1	2.13 ± 0.08
29 May	101 ± 3	175 ± 2	156 ± 6	< 19	235 ± 8	46 ± 5	63 ± 2	81 ± 4	12.7 ± 0.5	27 ± 1	50 ± 2	0.180 ± 0.007	7.2 ± 0.3	0.32 ± 0.01
30 May	85 ± 3	137 ± 1	107 ± 5	21.0 ± 0.8	299 ± 8	54 ± 1	71 ± 2	72 ± 5	10.5 ± 0.4	< SB	29 ± 1	0.127 ± 0.007	4.8 ± 0.2	0.34 ± 0.01
31 May	210 ± 10	311 ± 6	250 ± 10	42 ± 2	375 ± 1	103 ± 5	75 ± 2	170 ± 3	36 ± 1	106 ± 1	136 ± 5	0.163 ± 0.008	6.5 ± 0.3	0.54 ± 0.02
14 June	690 ± 10	680 ± 5	770 ± 30	20.9 ± 0.8	800 ± 10	320 ± 10	131 ± 4	423 ± 2	67 ± 2	136 ± 1	123 ± 5	1.29 ± 0.06	34 ± 1	1.80 ± 0.06
15 June	401 ± 2	470 ± 10	540 ± 20	20.9 ± 0.7	540 ± 10	210 ± 5	102 ± 3	251 ± 2	61 ± 2	133 ± 2	154 ± 6	2.01 ± 0.09	55 ± 2	1.82 ± 0.06
16 June	195 ± 1	243 ± 20	290 ± 10	20.9 ± 0.6	294 ± 4	133 ± 1	97 ± 4	125 ± 1	35 ± 1	80 ± 2	108 ± 5	1.78 ± 0.08	54 ± 2	0.67 ± 0.03
17 June	520 ± 20	610 ± 10	700 ± 30	< 19	660 ± 20	258 ± 1	110 ± 5	353 ± 9	65 ± 2	146 ± 1	141 ± 6	1.75 ± 0.09	52 ± 2	1.15 ± 0.06
18 June	680 ± 20	780 ± 30	740 ± 30	20.9 ± 0.8	870 ± 20	310 ± 10	138 ± 5	454 ± 3	65 ± 3	168 ± 7	132 ± 6	1.76 ± 0.05	51 ± 2	1.56 ± 0.06
19 June	610 ± 60	818 ± 9	850 ± 20	20.9 ± 0.9	780 ± 20	310 ± 30	165 ± 6	370 ± 10	63 ± 2	157 ± 7	100 ± 4	1.53 ± 0.07	46 ± 2	1.37 ± 0.05
20 June	234 ± 6	420 ± 20	490 ± 20	21.1 ± 0.8	469 ± 1	214 ± 1	198 ± 5	167 ± 9	42 ± 1	138 ± 1	116 ± 4	1.46 ± 0.06	41 ± 1	2.11 ± 0.08
02 July	430 ± 20	478 ± 9	550 ± 20	< 19	490 ± 9	218 ± 9	90 ± 4	269 ± 6	42 ± 1	100 ± 4	69 ± 2	0.83 ± 0.02	23 ± 1	0.93 ± 0.04
05 July	570 ± 30	550 ± 20	660 ± 20	< 19	750 ± 20	292 ± 9	126 ± 6	360 ± 10	54 ± 2	122 ± 2	75 ± 3	0.87 ± 0.05	24 ± 1	1.29 ± 0.05
06 July	408 ± 6	490 ± 6	570 ± 20	< 19	530 ± 10	212 ± 3	80 ± 4	276 ± 5	52 ± 2	109 ± 2	67 ± 2	1.32 ± 0.06	36 ± 1	1.16 ± 0.05
07 July	290 ± 10	324 ± 2	310 ± 10	< 19	350 ± 10	161 ± 5	80 ± 3	170 ± 10	27 ± 1	95 ± 6	52 ± 3	1.22 ± 0.05	34 ± 1	0.78 ± 0.03
10 July	235 ± 1	302 ± 1	380 ± 10	< 19	428 ± 1	146 ± 1	100 ± 5	157 ± 2	44 ± 1	30 ± 2	35 ± 2	0.77 ± 0.04	22 ± 1	0.74 ± 0.04
11 July	310 ± 20	280 ± 10	330 ± 20	< 19	390 ± 20	168 ± 10	77 ± 4	180 ± 10	35 ± 1	45 ± 2	31 ± 1	0.88 ± 0.03	28 ± 1	0.84 ± 0.03
14 July	143 ± 4	139 ± 1	175 ± 8	21.0 ± 0.8	199 ± 3	140 ± 10	109 ± 4	74 ± 1	21 ± 1	59 ± 1	59 ± 2	1.13 ± 0.04	27 ± 1	0.43 ± 0.02
15 July	223 ± 4	270 ± 10	316 ± 9	21 ± 1	381 ± 4	160 ± 1	117 ± 4	153 ± 2	36 ± 2	53 ± 5	50 ± 2	0.91 ± 0.03	24 ± 1	0.49 ± 0.03

SB: Sample Blank

Table 6S. Minor and trace element (Ba, Cr, Cu, Mn, Ni, Pb, Sn, Ti, V and Zn) concentrations in PM₁₀ samples. All the results are expressed in ng/m³.

	Ba	Cr	Cu	Mn	Ni	Pb	Sn	Ti	V	Zn
25 May	4.36 ± 0.07	< SB	7.5 ± 0.1	5.304 ± 0.007	0.95 ± 0.08	0.76 ± 0.01	2.3 ± 0.2	4.16 ± 0.08	0.27 ± 0.01	8.6 ± 0.3
26 May	4.8 ± 0.1	< SB	10.7 ± 0.5	5.384 ± 0.007	0.87 ± 0.07	0.88 ± 0.03	3 ± 1	3.33 ± 0.09	0.27 ± 0.01	8.6 ± 0.1
27 May	6.1 ± 0.7	0.59 ± 0.09	11.7 ± 0.4	6.3 ± 0.2	2.0 ± 0.4	1.7 ± 0.2	2.9 ± 0.2	7 ± 1	1.7 ± 0.1	14 ± 1
28 May	6.0 ± 0.2	1.23 ± 0.09	9.7 ± 0.9	6.63 ± 0.09	2.62 ± 0.02	2.27 ± 0.06	3.7 ± 0.3	6.7 ± 0.3	2.27 ± 0.03	13 ± 1
29 May	5.6 ± 0.8	0.042 ± 0.002	9.42 ± 0.09	5.63 ± 0.04	1.22 ± 0.02	0.79 ± 0.08	1.5 ± 0.1	4.4 ± 0.7	0.54 ± 0.03	17.0 ± 0.8
30 May	7 ± 1	0.199 ± 0.005	7.3 ± 0.3	5.9 ± 0.3	1.20 ± 0.04	0.54 ± 0.03	2.7 ± 0.3	4.0 ± 0.2	0.23 ± 0.01	22.8 ± 0.3
31 May	8.2 ± 0.3	1.26 ± 0.05	9.4 ± 0.3	8.95 ± 0.04	2.04 ± 0.03	1.22 ± 0.01	3.7 ± 0.1	7.2 ± 0.5	0.66 ± 0.03	18.1 ± 0.3
14 June	14.9 ± 0.1	6.9 ± 0.8	23.0 ± 0.2	30 ± 1	4.9 ± 0.5	7.35 ± 0.07	6.32 ± 0.09	22 ± 1	2.27 ± 0.04	33.7 ± 0.8
15 June	10.4 ± 0.3	1.93 ± 0.02	17.3 ± 0.4	34 ± 2	3.66 ± 0.06	6.1 ± 0.2	6.5 ± 0.3	12.6 ± 0.5	3.8 ± 0.1	23 ± 2
16 June	5.6 ± 0.3	0.089 ± 0.005	10.9 ± 0.2	9.03 ± 0.08	2.85 ± 0.06	2.73 ± 0.08	4.1 ± 0.4	5.4 ± 0.2	4.39 ± 0.05	9.0 ± 0.2
17 June	11.4 ± 0.3	3.25 ± 0.07	19.2 ± 0.3	21.67 ± 0.03	4.4 ± 0.1	4.75 ± 0.05	5.46 ± 0.08	13.0 ± 0.4	3.90 ± 0.07	22.4 ± 0.5
18 June	46.6 ± 0.6	6.0 ± 0.2	21.0 ± 0.7	22.6 ± 0.4	4.8 ± 0.1	4.6 ± 0.1	5.9 ± 0.4	20.6 ± 0.9	3.2 ± 0.1	25.6 ± 0.9
19 June	59 ± 3	5.5 ± 0.7	19.58 ± 0.02	20.9 ± 0.6	3.9 ± 0.2	5.0 ± 0.2	5.0 ± 0.3	20 ± 3	2.5 ± 0.1	49 ± 2
20 June	63 ± 5	3.1 ± 0.1	18.9 ± 0.4	33 ± 7	2.54 ± 0.03	3.2 ± 0.1	4.5 ± 0.2	7.70 ± 0.07	1.94 ± 0.04	43 ± 2
02 July	43.5 ± 0.8	3.6 ± 0.5	14.0 ± 0.5	13.93 ± 0.01	2.9 ± 0.1	3.76 ± 0.06	3.6 ± 0.3	12.9 ± 0.8	1.5 ± 0.1	40 ± 10
05 July	43 ± 1	4.5 ± 0.2	22.1 ± 0.5	21.2 ± 0.7	3.80 ± 0.09	4.4 ± 0.1	5.4 ± 0.2	16 ± 1	1.67 ± 0.08	28.1 ± 0.4
06 July	43 ± 1	3.4 ± 0.1	15 ± 1	20.9 ± 0.1	2.77 ± 0.09	3.5 ± 0.8	4.3 ± 0.6	17 ± 3	1.31 ± 0.07	37 ± 2
07 July	52.0 ± 0.3	1.92 ± 0.07	11 ± 1	19 ± 2	1.8 ± 0.2	3.50 ± 0.03	3.36 ± 0.03	9.6 ± 0.6	0.87 ± 0.01	36.2 ± 0.1
10 July	< SB	4.1 ± 0.1	14.67 ± 0.08	9.9 ± 0.2	2.2 ± 0.2	2.57 ± 0.02	4.10 ± 0.05	8.1 ± 0.2	0.66 ± 0.02	10.8 ± 0.1
11 July	< SB	4.7 ± 0.5	13.1 ± 0.2	11.6 ± 0.6	2.1 ± 0.3	3.0 ± 0.2	3.61 ± 0.08	10 ± 1	0.81 ± 0.05	13.9 ± 0.4
14 July	11.6 ± 0.1	1.48 ± 0.02	8.8 ± 0.2	8.1 ± 0.5	1.47 ± 0.01	2.26 ± 0.02	2.48 ± 0.03	5.5 ± 0.4	1.45 ± 0.01	13.6 ± 0.4
15 July	16.5 ± 0.4	2.54 ± 0.02	15.1 ± 0.8	9.20 ± 0.02	1.9 ± 0.1	2.37 ± 0.05	4.73 ± 0.07	6.8 ± 0.2	1.10 ± 0.01	18.6 ± 0.1

SB: Sample Blank

Table 7S. Trace element (As, Cd, Ce, Co, La, Mo, Tl and Zr) concentrations in PM₁₀ samples. All the results are expressed in pg/m³.

	As	Cd	Ce	Co	La	Mo	Tl	Zr
25 May	540 ± 10	34 ± 1	113 ± 8	36 ± 2	87 ± 2	178 ± 7	2.2 ± 0.2	334 ± 17
26 May	600 ± 40	30 ± 4	130 ± 9	25.3 ± 0.7	80 ± 3	217 ± 1	4.0 ± 0.6	340 ± 7
27 May	630 ± 30	35 ± 3	210 ± 20	141 ± 4	140 ± 10	290 ± 20	7.4 ± 0.7	420 ± 50
28 May	625 ± 7	58 ± 1	270 ± 10	168 ± 4	170 ± 10	380 ± 5	7.43 ± 0.03	318 ± 2
29 May	560 ± 20	34 ± 2	92 ± 3	47 ± 2	63.9 ± 0.5	256 ± 5	2.0 ± 0.2	280 ± 10
30 May	593 ± 6	23.6 ± 0.7	80 ± 5	48 ± 6	55 ± 4	450 ± 10	1.78 ± 0.08	510 ± 20
31 May	700 ± 30	129 ± 2	220 ± 10	74 ± 2	124 ± 5	458 ± 3	4.6 ± 0.2	650 ± 30
14 June	1300 ± 100	99 ± 2	770 ± 40	189 ± 8	590 ± 20	1040 ± 10	17.4 ± 0.4	1070 ± 50
15 June	1020 ± 40	90 ± 3	460 ± 10	99 ± 1	388 ± 9	710 ± 20	17.1 ± 0.6	700 ± 10
16 June	780 ± 20	49 ± 2	194 ± 9	50.2 ± 0.2	187 ± 1	485 ± 7	12.0 ± 0.5	380 ± 10
17 June	890 ± 10	69 ± 2	530 ± 20	1060 ± 20	382 ± 9	753 ± 7	16.9 ± 0.2	860 ± 10
18 June	590 ± 10	114 ± 3	618 ± 20	222 ± 3	412 ± 3	930 ± 30	16.3 ± 0.8	1020 ± 40
19 June	569 ± 1	88 ± 3	530 ± 20	210 ± 20	370 ± 10	960 ± 40	24.1 ± 0.9	1000 ± 100
20 June	413 ± 8	82 ± 2	111 ± 1	112 ± 1	119 ± 1	840 ± 20	26.0 ± 0.8	860 ± 10
02 July	345 ± 9	63 ± 3	352 ± 6	130 ± 3	258 ± 3	529 ± 4	10.3 ± 0.3	520 ± 20
05 July	444 ± 6	73 ± 4	450 ± 20	164 ± 5	400 ± 10	910 ± 30	11.7 ± 0.4	820 ± 80
06 July	560 ± 20	91 ± 5	250 ± 10	104 ± 2	320 ± 10	770 ± 50	14.6 ± 0.8	460 ± 40
07 July	490 ± 10	90 ± 2	109 ± 5	63 ± 5	186 ± 3	503 ± 7	15.3 ± 0.3	390 ± 10
10 July	383 ± 4	68 ± 2	85.6 ± 0.2	74 ± 3	85 ± 2	850 ± 20	12.3 ± 0.2	640 ± 10
11 July	390 ± 20	74 ± 4	130 ± 10	97 ± 7	150 ± 10	740 ± 40	14.5 ± 0.9	450 ± 40
14 July	280 ± 4	68 ± 3	< SB	38.6 ± 0.7	165 ± 3	420 ± 6	11.8 ± 0.3	260 ± 4
15 July	353 ± 7	79 ± 3	83 ± 1	95 ± 4	148 ± 4	680 ± 10	10.5 ± 0.2	530 ± 3

SB: Sample Blank

Table 8S: Lead isotope ratios (namely $^{204}\text{Pb}/^{206}\text{Pb}$, $^{206}\text{Pb}/^{207}\text{Pb}$ and $^{208}\text{Pb}/^{206}\text{Pb}$ ratios) for PM_{10} samples collected during start-up phase of the incinerator.

	$^{204}\text{Pb}/^{206}\text{Pb}$	$^{206}\text{Pb}/^{207}\text{Pb}$	$^{208}\text{Pb}/^{206}\text{Pb}$
	Mean \pm SD	Mean \pm SD	Mean \pm SD
25 May	0.0541 \pm 0.0005	1.1532 \pm 0.0003	2.1228 \pm 0.0006
26 May	0.0538 \pm 0.0004	1.1601 \pm 0.0002	2.1186 \pm 0.0004
27 May	0.0526 \pm 0.0004	1.1488 \pm 0.0002	1.8633 \pm 0.0009
28 May	0.0516 \pm 0.0006	1.1597 \pm 0.0009	1.8453 \pm 0.0012
29 May	0.0536 \pm 0.0004	1.1685 \pm 0.0005	2.0825 \pm 0.0012
30 May	0.0532 \pm 0.0001	1.1626 \pm 0.0006	2.0922 \pm 0.0001
31 May	0.0531 \pm 0.0001	1.1635 \pm 0.0006	2.1180 \pm 0.0005
14 June	0.0565 \pm 0.0002	1.1643 \pm 0.0009	2.0561 \pm 0.0018
15 June	0.0551 \pm 0.0006	1.1642 \pm 0.0003	2.0176 \pm 0.0003
16 June	0.0519 \pm 0.0003	1.1677 \pm 0.0005	1.9363 \pm 0.0001
17 June	0.0543 \pm 0.0006	1.1308 \pm 0.0002	2.0266 \pm 0.0008
18 June	0.0557 \pm 0.0002	1.1370 \pm 0.0009	2.0212 \pm 0.0014
19 June	0.0566 \pm 0.0002	1.1686 \pm 0.0001	2.0159 \pm 0.0025
20 June	0.0514 \pm 0.0006	1.1721 \pm 0.0003	1.8929 \pm 0.0041
02 July	0.0522 \pm 0.0004	1.1363 \pm 0.0009	1.9752 \pm 0.0007
05 July	0.0535 \pm 0.0003	1.1344 \pm 0.0011	2.0354 \pm 0.0015
06 July	0.0530 \pm 0.0008	1.1448 \pm 0.0012	1.9576 \pm 0.0043
07 July	0.0501 \pm 0.0004	1.2073 \pm 0.0005	1.8884 \pm 0.0015
10 July	0.0512 \pm 0.0003	1.1883 \pm 0.0007	1.9085 \pm 0.0002
11 July	0.0504 \pm 0.0004	1.1933 \pm 0.0008	1.8789 \pm 0.0039
14 July	0.0505 \pm 0.0003	1.1962 \pm 0.0005	1.9126 \pm 0.0014
15 July	0.0504 \pm 0.0001	1.2118 \pm 0.0009	1.8836 \pm 0.0006